



HAL
open science

Monitoring of natural oil seepage in the Lower Congo Basin using SAR observations

Romain Jatiault, Damien Dhont, Lies Loncke, Dominique Dubucq

► **To cite this version:**

Romain Jatiault, Damien Dhont, Lies Loncke, Dominique Dubucq. Monitoring of natural oil seepage in the Lower Congo Basin using SAR observations. *Remote Sensing of Environment*, 2017, 191, pp.258 - 272. 10.1016/j.rse.2017.01.031 . hal-04498632

HAL Id: hal-04498632

<https://hal.science/hal-04498632>

Submitted on 12 Mar 2024

HAL is a multi-disciplinary open access archive for the deposit and dissemination of scientific research documents, whether they are published or not. The documents may come from teaching and research institutions in France or abroad, or from public or private research centers.

L'archive ouverte pluridisciplinaire **HAL**, est destinée au dépôt et à la diffusion de documents scientifiques de niveau recherche, publiés ou non, émanant des établissements d'enseignement et de recherche français ou étrangers, des laboratoires publics ou privés.

1 **Monitoring of natural oil seepage in the Lower Congo Basin using**

2 **SAR observations**

3 Romain Jatiault ^{a, b*}, Damien Dhont ^a, Lies Loncke ^b, Dominique Dubucq ^a

4 ^a Total SA, Centre Scientifique et Technique Jean Feger (CSTJF), Avenue Larribau, 64018 Pau, France

5 ^b University of Perpignan Via Domitia, Centre de Formation et de Recherche sur les Environnements Méditerranéens (CEFREM), UMR 5110, 52 Avenue Paul

6 Alduy, 66100 Perpignan, France

7 *Corresponding author. University of Perpignan Via Domitia, Centre de Formation et de Recherche

8 sur les Environnements Méditerranéens (CEFREM), UMR 5110, 52 Avenue Paul Alduy, 66100

9 Perpignan, France. Tel.: +334 68 66 20 98

10 E-mail adresses: romain.jatiault@univ-perp.fr, romain.jatiault@total.com (R. Jatiault)

11 **Abstract**

12 Synthetic Aperture Radar (SAR) is a spaceborne tool allowing near real-time imagery over large
13 ground footprints of areas hundreds of kilometres wide. SAR also allows persistent observations
14 of the process of oil discharges, benefiting from (1) day and night observations, (2) independence
15 of cloud cover and (3) high revisiting frequencies. The interpretation of 82 SAR scenes over the
16 Lower Congo Basin for the 1994-2012 period allowed the recognition of 1400 natural seepage
17 slicks associated with 102 individual seep sites. We acquired an additional SAR data set with a
18 short revisit time over a selected prolific area. The data set consisted of 22 SAR scenes acquired
19 over a 10-day period, meaning a maximum revisiting period of 12 hours between subsequent SAR
20 acquisitions. The short-term approach shows that seepage slicks were detected with wind speeds
21 between 1.5 and 6.5 m/s (2.91 to 12.63 knots). Both long-term and short-term monitoring
22 evidences that seepage events are intermittent, with the occurrence rate of oil release ranging from
23 5 to 80%. Short-term monitoring shows that the seepage pace is independent between seep sites,
24 suggesting contrasted controlling factors. It also shows that the residence time of seepage slicks is
25 systematically shorter than 12 hours, which is far below reported values. Understanding the
26 seepage slick residence time is essential to provide an accurate estimation of the fluid flow and to
27 compute the volumetric outflow. The integration of in-situ mooring points measuring the current
28 velocity 10 m below the sea surface, in addition to local wind field and slick length, allowed us to
29 more accurately estimate the residence time of oil slicks at the sea surface before vanishing. The
30 results show that the sea surface residence time of oil slicks is limited to a few hours, with a
31 median value of 3h15min. These new residence time estimations allowed us to propose a
32 quantification of the regional oil output in the Lower Congo Basin, estimated at 4380 m³/year.
33 This area may therefore be considered as the world's third biggest oil-supplying province from
34 natural leakages.

35 **1. Introduction**

36 Natural discharges of hydrocarbon fluids occur in most of the world's petroleum basins
37 (Kvenvolden and Cooper, 2003; National Research Council, 2003; Kvenvolden and Rogers, 2005;
38 Etiope, 2015). Because of its sensitivity to centimetre wavelengths (e.g., McCandless and
39 Jackson, 2003), Synthetic Aperture Radar (SAR) is a remotely operated tool widely used in ocean
40 studies for the recognition of sea surface patterns. Satellites with an on-board SAR system are
41 used to detect natural liquid hydrocarbon seepage at the sea surface (Johannessen et al., 2000;
42 Espedal and Johannessen, 2000; MacDonald et al., 2002; Brekke and Solberg 2005; Garcia-
43 Pineda et al., 2009, Fingas and Brown 2014) in complement to spaceborne optical data
44 (MacDonald et al., 1993; Macdonald et al., 2002; Hu et al., 2009; Chen and Hu, 2014). The
45 presence of oil flattens the sea surface and significantly reduces the amount of energy
46 backscattered to the satellite (Fresnel specular reflection) compared to the surrounding free water.
47 Sea surface covered by oil seepage appears as black streaks on SAR images (Johannessen et al.,
48 2000; Espedal and Johannessen, 2000; Williams and Lawrence, 2002; Ivanov et al., 2007;
49 Zatygalova et al., 2007; Garcia-Pineda et al., 2009; Körber et al., 2014). Up to now, research on
50 sea surface manifestations of thermogenic seeps has focused on a few case studies, including the
51 Caspian Sea (Ivanov et al., 2007; Zatygalova et al, 2007), the Black Sea (Körber et al., 2014) and
52 the Gulf of Mexico (Garcia-Pineda et al., 2014, Macdonald et al., 2015). The SAR method also
53 serves as a primary tool for the evaluation of released volumes of heavy hydrocarbon discharges
54 (MacDonald et al., 1993; Mitchell et al., 2000; Garcia-Pineda et al., 2014), even if quantifications
55 may have been potentially underestimated with this technique (Hu et al., 2009; Garcia-Pineda et
56 al., 2010; Smith et al., 2014). Oil seep systems are usually accompanied by gas escapes (Solomon
57 et al., 2009; Hu et al., 2012) originating from the thermal cracking and the second methanogenesis
58 from anaerobic biodegradation (Head et al., 2003; Peters et al., 2007). For environmental
59 purposes, quantifying natural hydrocarbon escapes is therefore compulsory to understand their
60 implications on the global carbon budget. Understanding the amount of expelled hydrocarbon at

61 the regional scale along continental margins also presents great implications for petroleum
62 systems evaluation. The sea surface residence time of oil slicks is an important input parameter
63 for the quantification of oil output but still remains poorly documented due to low revisiting
64 frequencies of SAR data. The Lower Congo Basin is considered as an active petroleum province
65 where geophysical investigations of the seafloor have allowed the recognition of high-density
66 fluid flow features (Gay et al., 2003; Gay et al., 2006a, b, c; Gay et al., 2007; Andresen et al.,
67 2010; Andresen and Huuse, 2011; Anka et al., 2013) of probable thermogenic origin (Gay et al.,
68 2002; Gay et al., 2006b; Andresen 2012; Anka et al., 2013). Natural oil seepage slicks have been
69 recognised at the sea surface at the regional scale in the Lower Congo Basin from observation
70 using SAR images (Williams and Lawrence 2002; Dhont et al., 2013; Deffontaines et al., 2014)
71 confirming that this area is a major active thermogenic fluid releasing domain and an excellent
72 natural work site for studying regional fluid release dynamics and associated expelled
73 hydrocarbon volumes.

74 The aim of this paper is to combine short-term and long-term SAR monitoring to compare the
75 pace of thermogenic seeps distributed along the Lower Congo Basin and to quantify the volumes
76 of expelled hydrocarbons. The study comprises an extensive archive comprising 82 SAR scenes
77 acquired between 1994 and 2012 used to detect and map seepage slicks and to determine the
78 location of recurrent oil seep sites. From these long-term observations, we assessed the activity of
79 individual active seeps in order to quantify expelled oil volumes. To address the question of the
80 seep lifespan, we set up a short-term monitoring with the acquisition of 22 SAR scenes every 12
81 hours during 10 days over a specific area recognised as a major active seeping province. The
82 tasking of overlapping SAR scenes over an active seeping area with a half day revisiting period
83 constitutes a first order approach to study the recurrence and synchronicity of fluid discharges at a
84 regional scale. For the first time, this study allows us to compare simultaneously the activity of
85 several active oil seeping sites, benefiting from a minimum of two SAR scenes each day. The
86 comparison between the local wind fields derived from SAR data and the occurrence of oil slicks

87 also helps to improve our knowledge of the relationships between slick detection and weather
88 conditions. In addition, the assessment of short-term seepage pace is decisive to categorise the
89 active, dormant and passive seep sites for research teams and exploratory cruises.

90 **2. The Lower Congo Basin**

91 **2.1. Geological context**

92 The Lower Congo Basin is located in offshore Angola, in the southern part of the Congo Delta
93 (Fig. 1A). The study area is located on a passive margin resulting from the opening of the South
94 Atlantic domain initiated during the Early Cretaceous (Duval et al., 1991; Cainelli and Mohriak
95 1999; Browfield and Charpentier, 2006). During the Neocomian to Barremian, the development
96 of syn-rift lakes gave rise to the prolific mudstone source rocks of the Bucomazi formation
97 (Burwood 1999). During the late Aptian, the post-rift shallow environments allowed the
98 development of thick hypersaline deposits overlaying a sag basin under conditions of regional
99 thermal subsidence (Marton et al., 2004; Brun and Fort, 2004; Fort et al., 2004; Beglinger et al.,
100 2012). During the Albian, sedimentation was characterised by carbonate ramp development (Da
101 Costa et al., 2000; Anka et al., 2009; Beglinger et al., 2012). As thermal subsidence and
102 progressive basin deepening continued, post-rift salt tectonics triggered by high sedimentation
103 rates caused strong deformation of the overburden. Subsequent evolution of the margin was
104 controlled by salt tectonics. The study area is sub-divided into three main provinces (Fig. 1B): an
105 internal extensional area where the salt layer has been extremely thinned, a mid-slope transitional
106 province where post-salt sedimentary series have been translated towards the basin, and a
107 compressive domain consisting of a wide area dominated by severe deformation associated with
108 salt diapirism, followed by a basinward compressive toe with extensive salt napes (Brice et al.,
109 1982; Duval et al., 1991; Schoellkopf and Patterson, 2000; Marton et al., 2004; Brun and Fort,
110 2004; Anka et al., 2013). The seaward part of the basin deformed by salt tectonics is delimited

111 from the abyssal plain by a distal compressive salt front (Anka et al., 2009). Intra-saliferous basins
112 are infilled with turbidites and display an alternation of mudstone, claystone, shale and sandstone.

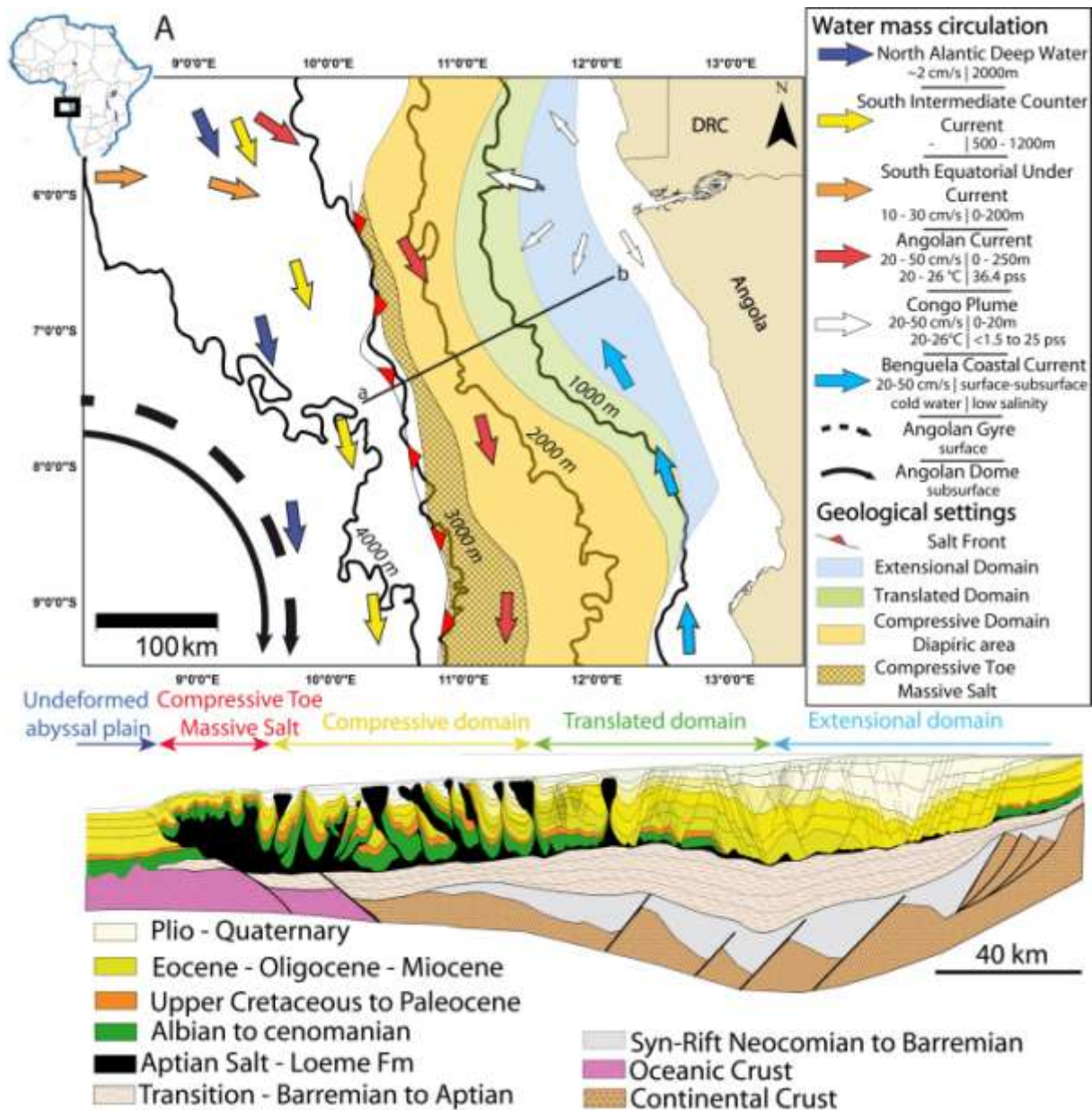
113 **2.2. Seafloor manifestation of fluid vents**

114 Geophysical investigations in the Lower Congo Basin report fluid escape features occurring as
115 focused depressions on the seafloor and sub-seafloor fluid migration chimneys (Gay et al., 2003;
116 Gay et al., 2007; Sahling et al., 2008; Anka et al., 2013). A large variety of pockmarks, defined as
117 seafloor expressions of focused fluid flows (King and McLean., 1970), have been described with
118 diameters varying from 30 m (Gay et al., 2007) up to 3150 m (Charlou et al., 2004; Ondreas et al.,
119 2005; Gay et al., 2006c). The Aptian salt withdrawal and associated gravitational deformation
120 greatly influenced the location of thermogenic seeps by creating efficient migration pathways
121 along salt flanks as demonstrated by several publications (e.g. Gay et al., 2007; Andresen et al.,
122 2010; Andresen and Huuse, 2011; Andresen, 2012). Wenau et al. (2014a, b) described active
123 escape features on the seafloor expelling gas bubble trains imaged from side scan sonar at the salt-
124 induced deformation front. From their fauna inventory, Jones et al. (2014) showed abundant
125 seafloor topographic reliefs, consisting of biodegraded oil which forms asphalt mounds with
126 diameters ranging from 0.5 to 50 m in the compressive salt province.

127 **2.3. Oceanographic context**

128 Understanding water mass movements is necessary for seepage studies because the strength of
129 underwater currents steers the trajectory of oil droplets in the water column, whilst sea surface
130 currents and wind determine the shape and lifespan of the oil slicks. The Fig. 1A displays a
131 summary of oceanographic transport along the Angolan coast. Surface water circulation is
132 prominently dominated by the southward Angolan Current (AC) (Moroshkin et al., 1970,
133 Hardman-Mountfort et al., 2003), which results from the combination of different surface and
134 subsurface currents, including the South Equatorial Under-Current (SEUC), Equatorial Under
135 Current (EUC), the steady state surface Angolan Dome (AD) (Doi et al., 2007), and the

136 subsurface Angolan Gyre (AG), which are respectively surface and subsurface permanent gyres
137 whose depth influence reach 500 m (Peterson and Stramma, 1991; Schneider et al., 1996; Holmes
138 et al., 1997; Stramma and England, 1999). The AC is bordered to the south by a frontal
139 convergence area with the Benguela current (Shannon, 2001), namely the Angolan-Benguela
140 Front Zone (ABFZ) (Lass et al., 2000; Boyer et al., 2000), roughly located along the Angolan-
141 Namibian frontier. However, the coastal and surfacing component of the Benguela Coastal
142 Current (BCC) bypasses the ABFZ, resulting in a current flowing towards the north along the
143 Angolan coasts (Hopkins et al., 2013). The Congo River outflow also inflects water circulation in
144 the northern area. Seasonal variations are characterised by two warm periods from February to
145 April and from September to November (Hardman-Mountford et al., 2003), alternating with two
146 cold periods characterised by strong upwellings. Intermediate water circulations are controlled by
147 the extension of the SICC to the south (Southern Intermediate Countercurrent) for water depths
148 comprised between 500 and 1200 m (Stramma and England, 1999; Stramma and Scott, 1999).
149 The main orientation of deepwater currents along the Angolan coast is controlled by the North
150 Atlantic Deep Water known to occur at 2000 m depth (NADW; Stramma and England, 1999;
151 Arhan et al., 2003) and flowing to the south at 2 cm/s (Lynn, 1971).



152

153 **Fig. 1. A:** Location map of the study area (see the African map within the black frame in the top
 154 left corner) superimposed with an overview of main oceanic currents and geological settings. The
 155 orientation of coloured arrows represents the directions of the hydrodynamic components of the
 156 basin. The characteristics of each current, including velocity, depth influence, temperature and
 157 salinity, appear in the legend when available. **B:** Geological cross-section of the Lower Congo
 158 Basin (a-b on Fig. 1A) including pre-rift, syn-rift, transitional and post-rift series (modified from
 159 Guilbot et al., 2012). See location of the section from the black line in Fig. 1A.

160 **3. Dataset and methods**

161 **3.1. SAR acquisition parameters for oil slick detection**

162 Synthetic Aperture Radar (SAR) is sensitive to centimetre-scale capillary waves induced by the
163 local wind at the sea surface (Franceschetti et al., 2002; McCandless and Jackson, 2003). Oil
164 surfactants smooth the sea surface and significantly reduce capillary waves, which triggers a
165 contrast in roughness between oil-covered areas and free water. A minimum wind speed is
166 required to trigger capillary waves and therefore to identify seepage slicks. The lower wind speed
167 limit for seepage slick detection varies between case studies and authors, from 1.5 m/s (Skrunes,
168 2014, Fingas and Brown, 2014), 2-3 m/s (Espedal and Wahl, 1999; Johannessen et al., 2000;
169 Girard-Arduin et al., 2005, Brekke and Sölberg, 2005) to 3.5 m/s (Garcia-Pineda et al., 2009). In
170 case of strong winds, natural oil slicks are also affected by capillary waves, which prevents the
171 detection of oil at the sea surface. Seepage slicks from natural discharges are considered to be
172 detectable up to 6-7 m/s (Bern et al., 1992; Espedal and Wahl, 1999). Some authors consider that
173 thicker slicks can be identified for higher wind speeds (Alpers and Espedal, 2004; Brekke and
174 Sölberg, 2005; Körber et al., 2014). In addition to the sea surface currents, it is assumed that 3%
175 of the wind speed accounts for the oil slick drift velocity (Bern, 1992; Espedal and Wahl, 1999;
176 Kim et al., 2014). Previous studies demonstrated that short wavelengths of the X- (2.5 to 3.75
177 cm), C- (3.75 to 7.5 cm) and Ku-bands (1.6 to 2.5 cm) are more efficient in detecting oil slicks at
178 the sea surface (Gade et al., 1998; Espedal and Wahl, 1999; Espedal and Johannessen, 2000;
179 Johannessen et al., 2000; Alpers and Espedal, 2004; Brekke and Sölberg, 2005; Girard-Arduin et
180 al., 2005; Skrunes, 2014). According to Bragg's reflection theory, the backscattered signal
181 decreases with increasing incidence angles between 20° to 70° (Alpers and Espedal, 2004). Ideal
182 incidence angles for slick detection range from 20° to 45° (Girard-Arduin et al., 2005; Brekke and
183 Sölberg, 2005; Garcia-Pineda et al., 2010). Vertical SAR polarisation (VV) is the most efficient
184 mode to detect oil slicks at the sea surface (Brekke and Solberg, 2005).

185 **3.2. SAR dataset**

186 **3.2.1. Long-term acquisitions**

187 Satellite SAR sensors are deployed on polar orbiting platforms, which enables worldwide
188 observations with a rapid repeat rate. The SAR operational mode allows day and night imagery,
189 regardless of cloud cover, which is one of the main advantages compared to passive optical
190 imagery. In order to find oil seep sites, we gathered a collection of 82 SAR images from different
191 satellite sensors (Fig. 2A). Archive data acquired from 1994 to 2012 were used to detect recurrent
192 oil slicks and afterward to identify the sea surface location of natural oil seepage.

193 The dataset provided by the European Space Agency (ESA) is composed of ASAR data
194 (Advanced Synthetic Aperture Radar) acquired in Image Mode Precision (IMP) by the European
195 Remote Sensing satellites (ERS 1 and 2) between 1994 and 2001 and Wide Swath Mode (WSM)
196 Envisat scenes acquired between 2002 and 2012, both operating in C-Band (Table 1). We
197 complemented this dataset with RADARSAT, TerraSAR-X and Cosmo-SkyMed data. The map
198 of SAR coverage density varies between 40 to 70 scenes (Fig. 2A). SAR scenes were converted
199 from N1 raw format to 8-bit geoTiff format, displayed in greyscale for visual interpretation with
200 GIS software (ArcInfo, ESRI). Scenes were kept speckled to preserve whole details. We applied
201 linear stretching to counterbalance signal loss with increasing incidence angle from the orbital
202 path.

203 **Table 1**

204 SAR data used for oil slick mapping during both long-term and short-term monitoring.

Satellite/ Sensor	Band/ Wavelength	Pixel Spacing (m)	Amount of SAR data	
			Long-term monitoring (1994 - 2012)	Short-term monitoring (12 - 22/10/2012)
Envisat /WSM	C (5.8 cm)	75	46	0
ERS/IMP	C (5.8 cm)	12.5	17	0
Cosmo-SkyMed	X (3.1 cm)	3-15	13	15
TerraSAR – X	X (3.1 cm)	20	2	4

RADARSAT-2	C (5.3 cm)	25-50	4	3
-------------------	-------------------	--------------	----------	----------

205 **3.2.2. Short-term monitoring**

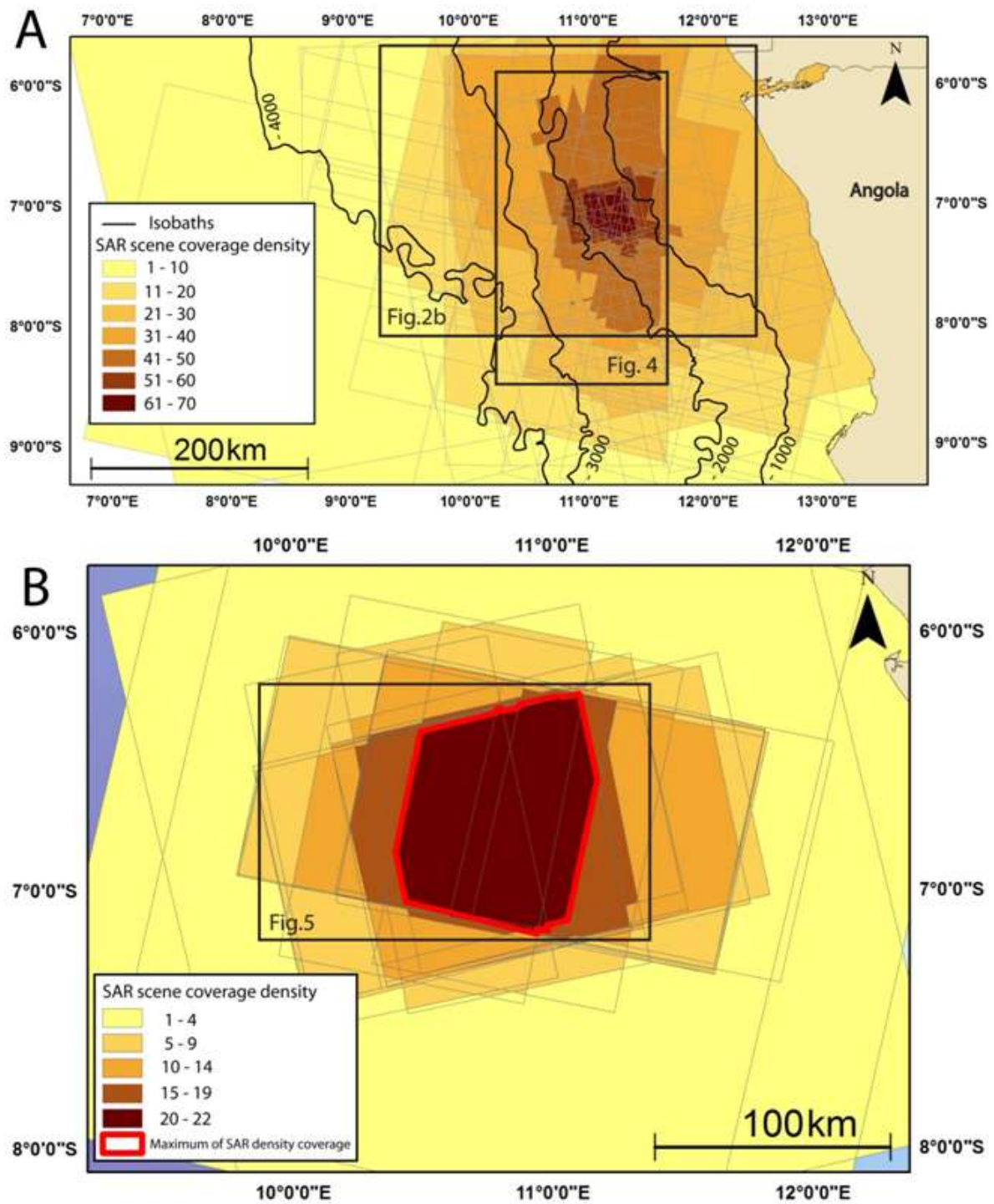
206 In order to investigate the seepage recurrence, synchronicity and lifespan on sea surface, we
207 performed a short-term monitoring based on the tasking of SAR images during a restricted period
208 of 10 days. We focused this monitoring on the area recognised for the largest amount of expelled
209 oil, located 135 km from the Angolan coast to the southwest of the mouth of the Congo River
210 (Fig. 2B). Tasking of 22 satellite images during 10 days provided at least one image every 12
211 hours (Table 2). The dataset consists of a combination of X-band (TerraSAR and Cosmo-
212 SkyMed) and C-band (RADARSAT) data. The radar density coverage constructed from the stack
213 of multi-temporal images varies spatially, including a central area of maximum coverage density
214 imaged by a series of at least 20 images out of the 22 tasked.

215 **Table 2**

216 Listing and characteristics of SAR scenes acquired during short-term monitoring

Scene number	Date (dd/mm/yyyy)	Time (hh:mm)	Sensor	Scene number	Date (dd/mm/yyyy)	Time (hh:mm)	Sensor
1	12/10/2012	05:40	Cosmo-SkyMed	12	18/10/2012	05:22	Cosmo-SkyMed
2	13/10/2012	04:58	RADARSAT - 2	13	18/10/2012	16:47	Cosmo-SkyMed
3	13/10/2012	16:53	Cosmo-SkyMed	14	18/10/2012	17:37	TerraSAR - X
4	13/10/2012	17:28	TerraSAR - X	15	19/10/2012	05:40	Cosmo-SkyMed
5	15/10/2012	05:06	TerraSAR - X	16	19/10/2012	16:47	Cosmo-SkyMed
6	15/10/2012	05:40	Cosmo-SkyMed	17	20/10/2012	04:54	RADARSAT - 2
7	15/10/2012	16:41	Cosmo-SkyMed	18	20/10/2012	16:35	Cosmo-SkyMed
8	16/10/2012	05:34	Cosmo-SkyMed	19	21/10/2012	04:58	TerraSAR - X
9	16/10/2012	17:42	RADARSAT - 2	20	21/10/2012	05:28	Cosmo-SkyMed
10	17/10/2012	05:34	Cosmo-SkyMed	21	21/10/2012	16:53	Cosmo-SkyMed
11	17/10/2012	06:53	Cosmo-SkyMed	22	22/10/2012	06:53	Cosmo-SkyMed

217



218

219 **Fig. 2.** A. Map of coverage density of Synthetic Aperture Radar scenes from 1994 to 2012. B.
 220 Coverage density of Synthetic Aperture Radar tasked during the short-term monitoring. The
 221 maximum coverage density of SAR scenes tasked during short-term monitoring occurs within the
 222 red polygon outline and covers 6736 km² with a water depth ranging from 1000 to 2750 metres.

223 3.2.3. *Wind and current assessments*

224 In order to observe the wind effect on slick detection, we compared the regional wind field with
225 the number of slicks detected and their size with the local wind field extracted at the location of
226 the oil slicks. Real-time wind field measurements are not available over the study area, hence we
227 used the regional wind field provided by the European Centre for Medium-Range Weather
228 Forecasts (ECMWF). The wind field is calculated every 6 hours with a spatial resolution of the
229 grid of $1/8^\circ$ (~14 km). The forecasted wind field has been averaged over 24 hours for better
230 comparison with the number of slicks detected in each image. In order to observe small-scale
231 variations of the wind field, we assessed the local wind from SAR scene derivation with the
232 scatterometer technique. Spatial resolution is 1150 m with a maximum speed uncertainty of 2 m/s
233 and 15° in direction (for details see Johannessen et al., 2000 and Zecchetto, 2015). The wind
234 dataset is composed of discrete data including forecasts and SAR-derived wind fields which
235 represents a certain limit for the understanding of the wind effect on slick dissipation between two
236 SAR acquisitions.

237 The current velocity is measured from ADCP (Acoustic Doppler Current Velocity) tools that use
238 particle displacement to quantify current speed (Rowe and Yound 1979; Gordon and RDI, 1996).
239 The data were collected during 6 months of mooring between January 2009 and July 2009 at a
240 depth of 10 m below the sea surface. The current velocity was not available during short-term
241 monitoring, but the integration of predated mooring data represents a good proxy to approach the
242 current velocity distribution.

243 **3.3. Identification of natural leakages at the sea surface**

244 Sea surface smoothing may be induced by a wide collection of look-alike seep features. Table 3
245 sums up look-alikes found during SAR scene interpretation.

246 **Table 3:**

247 Overview of look-alike features detected on SAR scenes and dismissal features

Look-alike type	Origin	SAR features	Dismissal method	References
Low Wind Areas	Insufficient wind speed to trigger capillary waves	Extensive dark patches	Masking of the affected region	Espedal and Wahl (1999)
Bioturbations	Surface covered area smoothes the sea surface	Threadlike extensive and scattered films	Masking of the affected region or SAR scene dismissal	Gade et al. (1998) Espedal and Johannessen (2000)
Boat spill	Ship hold cleaning	Straight slick caused by moving source, shining point at boat location	Slick mapping with appropriate "spill" rank attribution	Espedal and Wahl (1999)
Platform/ Pipeline spills	Accidental/operational production pollution	Petroleum infrastructure data integration (IHS) and shining platform	Slick mapping with appropriate "spill" rank attribution	Trivero and Biamino (2010)
Rain cells	Local opposite winds at the edge of rain cells cause roughness wipeouts	High roughness values in the internal cell area compared to free water and rounded features	Masking of the affected region	Espedal and Johannessen (2000)
Solitons or Internal waves	Decrease backscattered energy associated with wave-related slopes	Multiple parallel trends interspersed by greater backscattered values	Visual dismissal	Jackson et al. (2013)

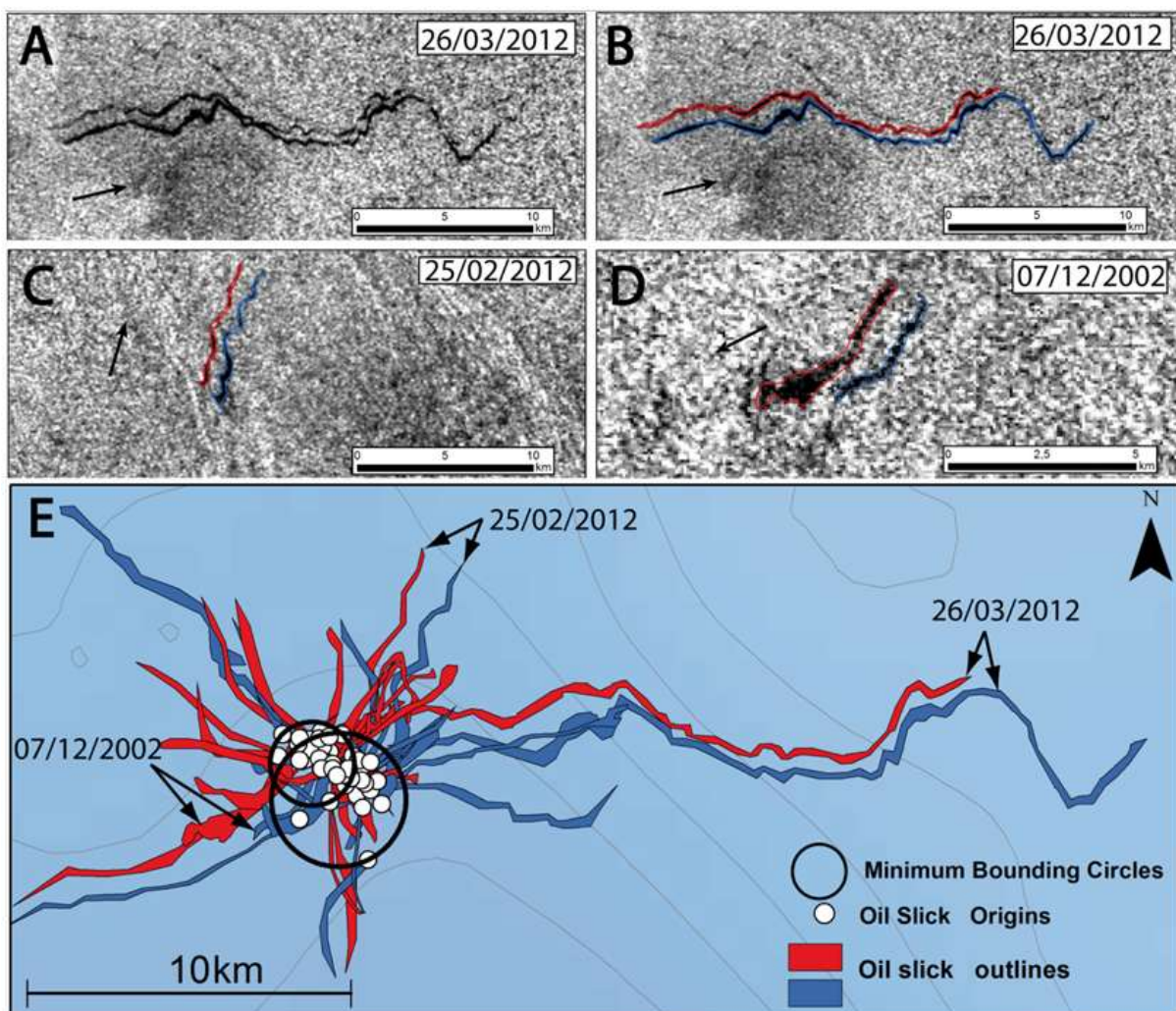
248

249 Petroleum infrastructure database integration (IHS) helps to discard leakage originating from
250 pipes and/or petroleum platforms. In addition, boats or platforms appear as shiny diffracting
251 points on SAR data, which make a distinctive feature compared to natural slicks. Spills from
252 anthropogenic activities represent about 15% of the total surfacing oil in this study. Rain cells and
253 solitons were occasional, in contrast to bioturbations which forced us to dismiss about 20% of
254 SAR scene collection. Regions of SAR scenes containing low wind areas, rain cells or
255 bioturbations were removed from the data collection to preserve the SAR coverage density which
256 is used to quantify the seepage activity. The shape of natural oil slicks is induced by the strength
257 and orientation of the wind and surface currents (Espedal and Wahl, 1999). Wind and surface
258 currents induce short-term variations of sea surface motion. The sinuosity of black patterns is a
259 first-order criterion to detect oil content slicks (Fig. 3 A - D). Sharp radiometric contrast between
260 oil-covered areas and the surrounding free water correspond to the sideward detectable edge of the

261 slicks and allowed us to identify the extent of individual seepage slicks (see examples in Fig. 3 A
262 and B). Computer-based automatic picking (Brekke and Solberg, 2005; Garcia-Pineda et al.,
263 2009) certainly provides a quick way to delineate dark features but is still not able to distinguish
264 natural seepage from anthropogenic pollutions or look-alikes (Suresh et al., 2013). Garcia-Pineda
265 et al. (2009) showed that the classification using neuronal networks between dark areas and free
266 water is equivalent to manual picking. In our case, visual interpretation is more powerful, as the
267 input of the photo-interpreter allows a confidence rank attribution which prevents the over-
268 interpretation of dark features. Therefore, we based our interpretation on manual picking instead
269 of computer-based automatic detection. We compiled on a map the outlines of each high-
270 confidence slick identified on each SAR image (Fig. 3E). Once mapped, diverging black streaks
271 evidence active seeping areas of thermogenic fluids (Kornacki et al., 1994; MacDonald et al.,
272 1996; de Beukelear et al., 2003; Zatyagalova et al., 2007; Garcia-Pineda et al., 2010; Garcia-
273 Pineda et al., 2014; Körber et al., 2014). The centre of each diverging structure corresponds to the
274 probable impact area of the fresher oil droplets at the sea surface. The Oil Slick Origin (OSO,
275 Garcia-Pineda et al., 2010; Körber et al., 2014) is visually drawn for each seepage slick from the
276 location of the proximal detectable edge of the slick to the seeping area (see white dots in Fig.
277 3E). Diverging slicks allowed us to sort seepage slicks and associated OSOs between recurrent
278 seep sites. We associated nearby and recurrent double-pattern slicks as being associated with two
279 different seep sites (Fig. 3).

280 From the location of each OSO, we computed the kernel density with the ArcGIS toolbox in order
281 to better display areas of active seepage. We also calculated the geometric mean centres (Garcia-
282 Pineda et al., 2010) for each diverging structure, corresponding to mean values of each OSO
283 location. The spatial dispersion of the OSOs generated by a single seep and detected in multiple
284 SAR images is related to the horizontal deflection of the oil plume through the water column. We
285 drew the minimum size circles encompassing each single OSO expelled from individual seep sites
286 to evaluate the offset range values generated by underwater deflection (Garcia-Pineda et al., 2010)

287 by using the minimum bounding geometry tool of the ArcGIS toolbox (Fig. 3E). The radius
288 serves as a proxy to quantify the horizontal deflection of oil droplets in the water column when
289 rising towards the sea surface. We also computed the ratio between the number of oil slicks
290 detected and the SAR scene coverage density, namely the occurrence rate, which gives an
291 indication of the frequency and release activity of each seep. Compared to SAR data coverage,
292 seep sites with high occurrence percentage frequently expel oil slicks, conversely to the low
293 occurrence percentage that corresponds to weaker seeping sites with few slicks detected during
294 the monitoring interval. We assessed the average oil volume at the sea surface from the method
295 developed by MacDonald et al. (2015), who gridded their area and considered the total surfacing
296 volume divided by the SAR coverage density for each cell.



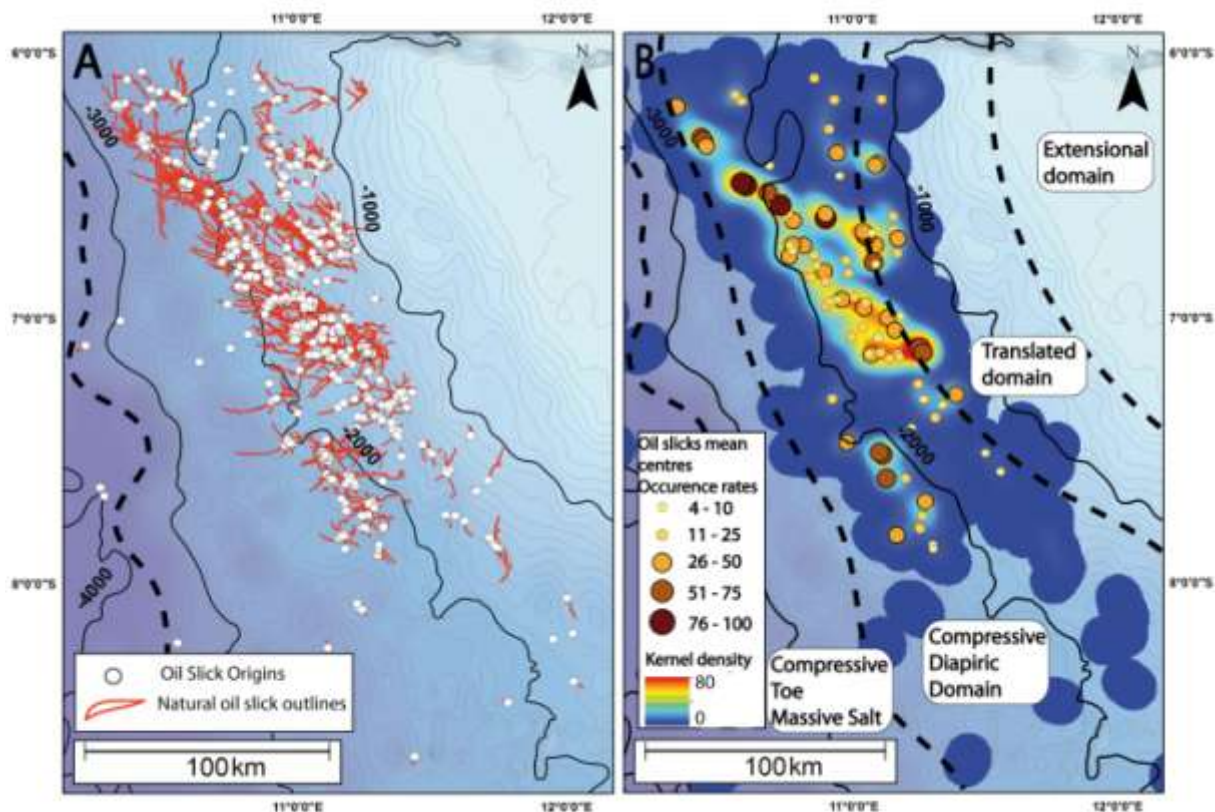
297

298 **Fig. 3.** A. Extract from SAR WSM scene dated 26/03/2012. Grey speckled background represents
299 backscattered energy from sea surface free water. Black streaks depict the location of seepage
300 slicks. B. Same SAR image extract complemented with manual picking. C and D. ASAR WSM
301 SAR sub-scenes respectively dated 25/02/2012 and 07/12/2002 superimposed with manual
302 picking of oil slicks. The three different SAR extracts overlap at a common spatial location. Black
303 arrows show the flow direction of surface currents during SAR scene acquisition. E. Compilation
304 map of oil slick outlines mapped from the entire dataset, including slicks displayed in A., B., C.
305 and D. at two major seep sites. All scenes are provided by the European Spatial Agency (ESA).

306 **4. Oil seep analysis and results**

307 **4.1. Long-term observations**

308 We mapped a total of 1600 oil slicks interpreted from the analysis of the 82 SAR data over 18
309 years. The integration of the IHS international exploration & production database and the
310 recognition of diffracting points associated with the boat or platform location allowed us to
311 remove about 200 slicks associated with anthropogenic activities. The remaining 1400 seepage
312 slicks are displayed in Fig 4A. Among them, 1240, i.e. 90%, of the slicks are recurrent, forming
313 diverging patterns on the compilation map. The length of the slicks varies from a few hundred
314 metres to 45 km. We recognised 102 active seep sites whose geometric mean centres are
315 displayed in coloured dots in Fig. 4B. The water depth of the seeping province ranges roughly
316 from 1100 to 2600 m at a distance of 130 to 200 km from the Angolan coastline. Active seep sites
317 are distributed all along the southern part of the Congo Basin over an area of 21,000 km². The
318 seeping province is well delimited from the basinward edge of the translated province and mainly
319 included in the compressive province associated with salt diapirs (Figs. 1 and 4). Occurrence rates
320 range between 5% for the weakest seeps and 80% for the most active (Fig. 4B), suggesting that
321 the flux of fluid differs between seep sites.

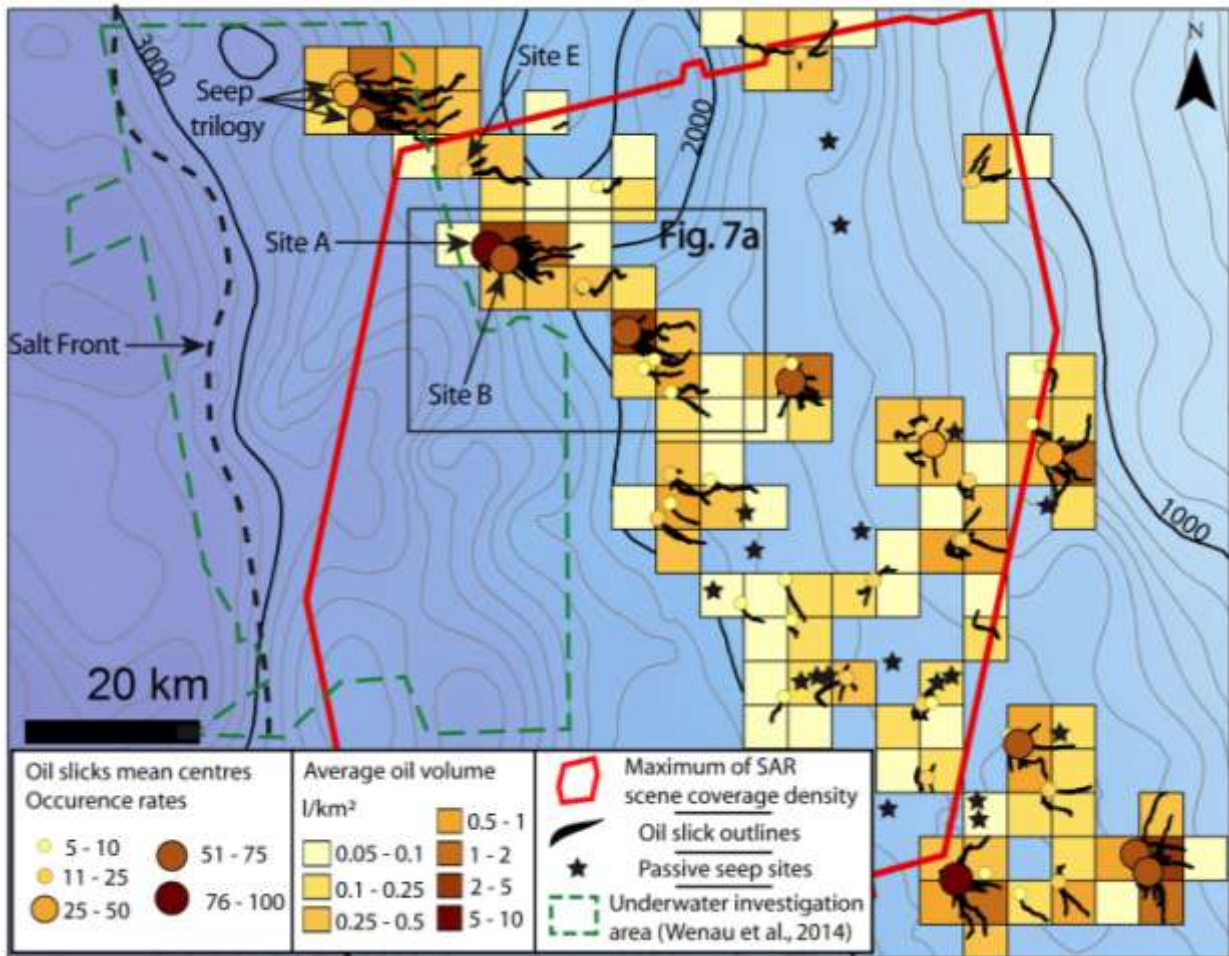


322
 323 **Fig. 4.** A. Compilation map of oil slick outlines in red polygons superimposed with Oil Slick
 324 Origins in white dots (see details in text). B. Kernel density computed from the density of seepage
 325 slicks. Coloured dots show the location of geometric mean centres of OSOs. The dashed black
 326 lines indicate the boundaries of each province related to the salt tectonics presented in Fig. 1B.

327 4.2.Short-term monitoring

328 4.2.1. *General observations*

329 We identified a total of 231 high-confidence oil seepage slicks from the interpretation of the 22
 330 tasked scenes. The locations of recurrent seep sites are consistent between the two monitorings.
 331 Recurrent slicks during short-term monitoring are associated with 53 seep sites identified from
 332 long-term monitoring (coloured dots in Fig. 5 - see location in Fig. 2). A total of 102 oil seep sites
 333 were mapped from long-term monitoring, suggesting that about 50% of seeping sites were passive
 334 during short-term monitoring (black stars in Fig. 5).



335

336 **Fig. 5.** Compilation map of oil slick outlines (black polylines) mapped from SAR scenes tasked
 337 during short-term monitoring and focused on the maximum coverage density area (see location in
 338 Fig. 2A). Coloured dots represent geometric mean centres of OSOs expelled from individual seep
 339 sites. Size and colours correspond to the occurrence percentages. Inactive seepage site locations
 340 during short-term monitoring are displayed as black stars. The salt tectonic boundary is displayed
 341 as a black dashed line. Background continuous lines are 100 m isobaths.

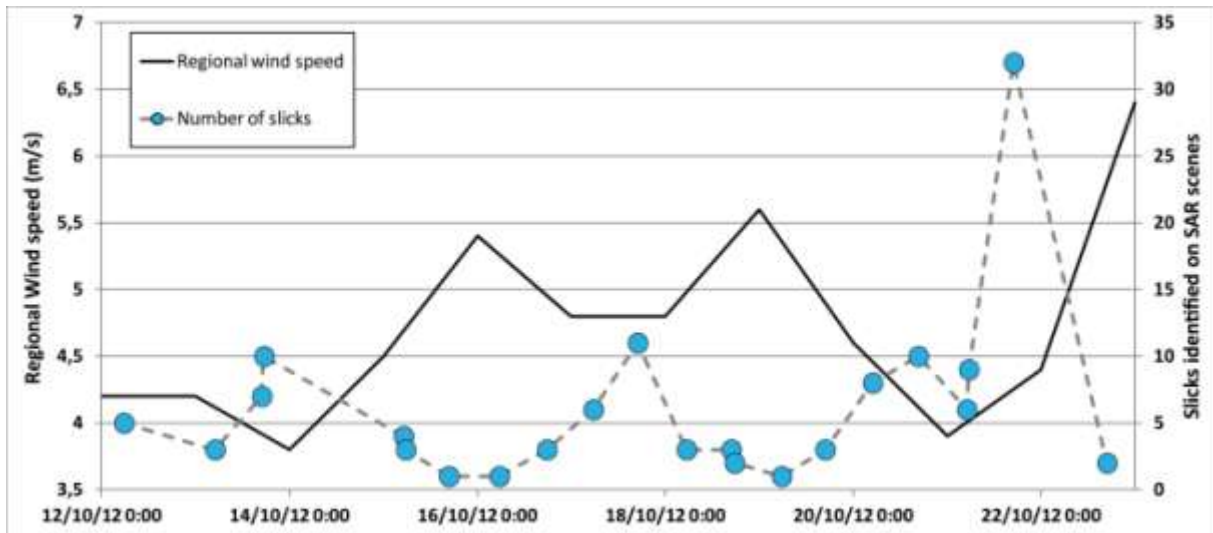
342

343 The area of highest radar coverage, defined as the area imaged by a minimum of 20 images out of
 344 the 22 tasked scenes, encompasses the 51 seeping sites observed during long-term monitoring
 345 (inside the red frame in Fig. 5).

346 In this area, 130 slicks with lengths varying from 1000 to 16,000 metres are associated with 33
347 geometric mean centres or active sites (Fig. 5). The spatial spreading of OSOs retrieved from the
348 computation of minimum bounding circles for each seep sites provides the estimation of the
349 deflection offset in the water column. The spatial dispersion of surfacing slick areas varies
350 between 80 and 1020 m, which remains low compared to the water depth of the seeping province
351 (from 1100 to 2600 m). As shown by the Fig. 1, the regional hydrodynamics involves multiple
352 oceanic components with various speed and depth influences. The horizontal deflection of oil
353 droplets in the water column is directly influenced by this hydrodynamic complexity. The linear
354 law between the water depth and the horizontal deflection established in the Gulf of Mexico
355 (Garcia-Pineda et al., 2010) does not apply for the Lower Congo Basin. As a matter of fact, the
356 greatest OSO dispersion values account for shallower areas in this study where the AC meets the
357 BCC's influence, probably resulting in greater current variability, whereas the deepest seep areas
358 are associated with restricted OSO spatial spreading.

359 4.2.2. *Correlation with the wind field*

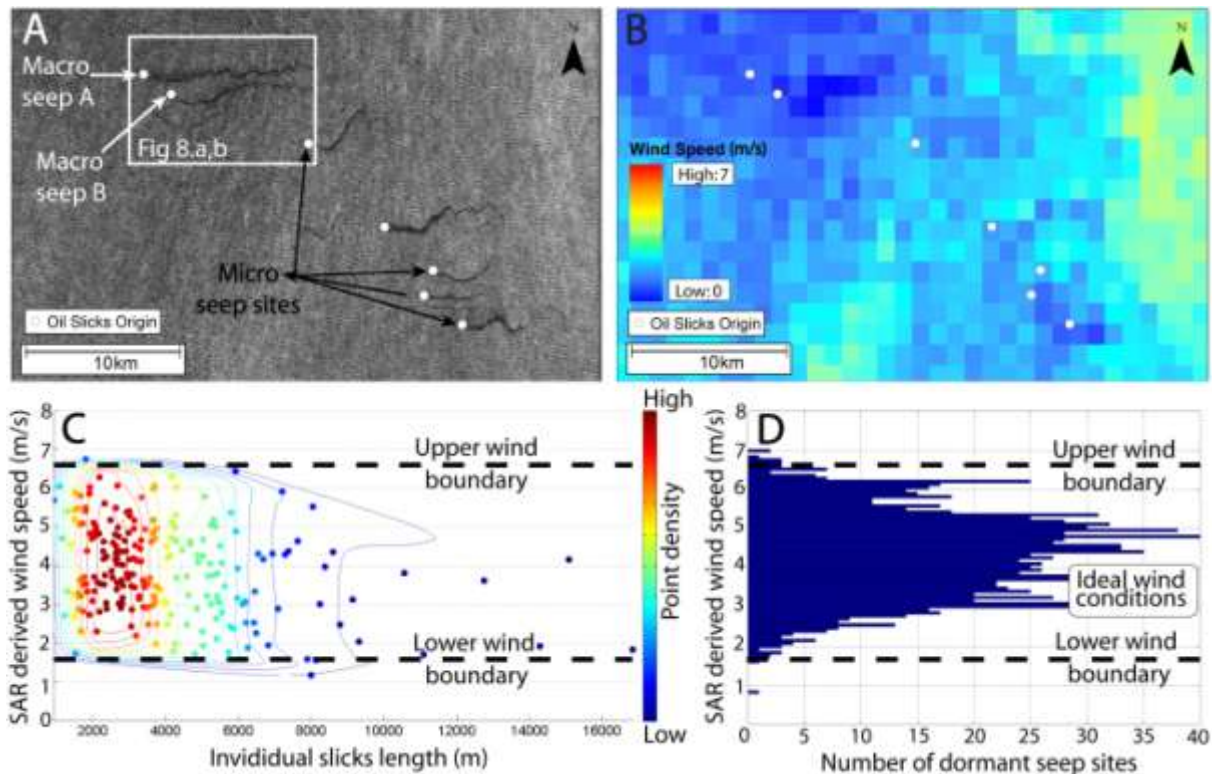
360 The study of seepage recurrence requires good knowledge of the wind speed to ensure the
361 consistency of the detection. As a first approach, we used the wind speed field forecasted at the
362 regional scale (ECMWF) to confirm that weather conditions were suitable all along the 10-day
363 acquisition period (Fig.6). The reported values of suitable wind speed for the detection of oil
364 slicks (Espedal and Wahl, 1999; Alpers and Espedal, 2004; Girard-Arduin et al., 2005; Brekke
365 and Sölberg, 2005; Garcia-Pineda et al., 2009; Fingas and Brown, 2014) confirm that the weather
366 conditions were suitable during short-term monitoring (from 3.7 to 6.5 m/s (Fig. 6) for the
367 recognition of oil slicks on SAR data.



368

369 **Fig. 6.** Superimposed graphs of modelled regional wind speed (ECMWF) displayed in black line
 370 and the number of slicks in the high-density SAR coverage area.

371 The two curves displaying the wind speed and the number of slicks show an anti-correlation,
 372 where higher wind speeds correspond to fewer detected slicks and vice versa. The curve
 373 displaying the number of detected slicks through time reveals three peaks characterised by an
 374 increase of the number of detected slicks (scenes 3 to 4, scenes 9 to 11, scenes 17 to 21 - see
 375 Table 2). These periods are interspersed by stages of low detection of slicks on SAR scenes
 376 especially at the following scenes: 5 to 8, and 12 to 16. These stages correspond to periods of
 377 regional wind speed intensification.



378

379 **Fig. 7.** A. Extract from the SAR scene dated 21 October 2012, 16:53 (scene 21). Black streaks
 380 show the location of oil slicks at the sea surface. B. Local wind values are retrieved from SAR
 381 scene derivation at the locations of OSOs displayed as white dots. C. Plot of the length of
 382 individual slicks and the local wind speed value at the location of OSOs. The colour of the dots
 383 ranging from red to blue respectively represents high to low point density. D. Histogram of the
 384 distribution of local wind values at the location of recurrent oil seeping areas revealed from long-
 385 term monitoring and measured during dormant stages in short-term monitoring. The vertical black
 386 dashed lines correspond to the probable ideal boundaries for seepage slick detection.

387 Even though the modelled wind provides a regional assessment of weather conditions, the
 388 applications related to local wind quantification remain questionable. Therefore, in order to
 389 quantify more accurately the ideal weather conditions for slicks in the study area, we integrated
 390 the local wind measurement extracted from SAR scenes from the scatterometer technique at the
 391 location of seepage slicks (Fig. 7A, B). Local wind values vary between 1.5 and 6.5 m/s at the

392 slick locations (Fig. 7C). This observed detectability agrees with lower and upper values reported
393 in the literature.

394 The information related to the population density of slick lengths shows that most of the slicks
395 (137 out of 231) were detected with lengths ranging from 1000 to 4000 metres. The population
396 density progressively decreases with the increase of the slick length. Slicks longer than 8000 m
397 were occasional and exclusively associated with local winds between 2 to 4 m/s, meaning that no
398 elongated slicks were detected with wind speeds above 4 m/s during the 10 days of monitoring
399 (Fig. 7C).

400 We then plotted the number of dormant seep sites on the SAR-derived winds (Fig. 7D).
401 Considering that ideal wind values range from 1.5 to 6.5 m/s in the study area, dormant seep
402 phases clearly occur during periods of ideal wind conditions. Only a restricted portion of dormant
403 seep sites (~5%) occur outside the ideal detection boundary conditions (Fig. 7D). This shows that
404 the disappearance of slicks at recurrent seep sites is associated with short-term intermittence.

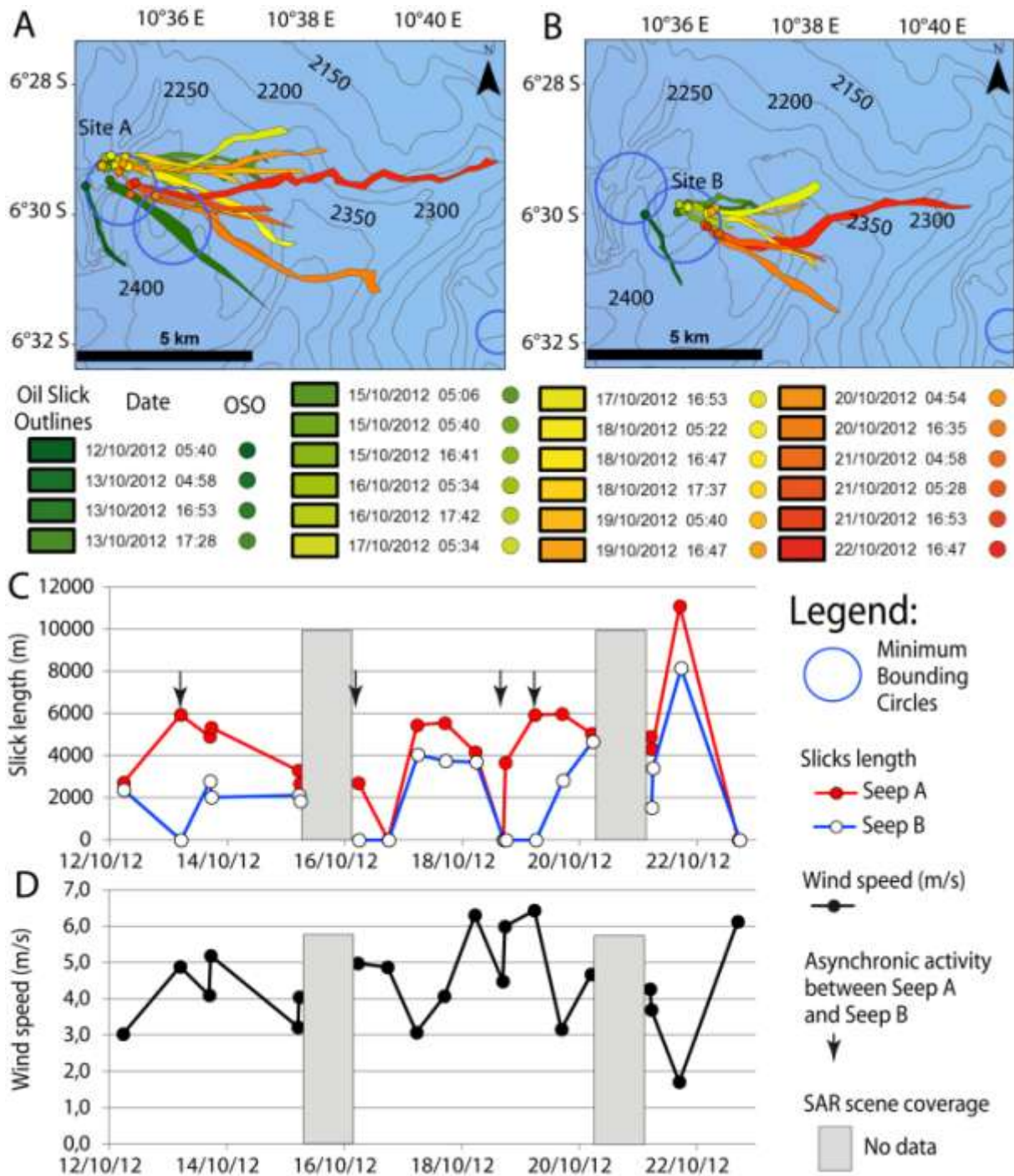
405 4.2.3. *Macro-seepage sites*

406 We defined macro-seepage sites as prolific leaking spots with occurrence rates above 50%.
407 Within the area of SAR maximum coverage density, the acquisition of SAR data simultaneously
408 at the nearby major seep sites allowed us to study the seepage pace for major seep sites during
409 short-term monitoring. Seep sites A and B are distinct seepage sites, as the identification of
410 recurrent double-pattern slicks allowed us to distinguish slicks expelled from one site to the other
411 (Fig. 7A). The two sites are only 2250 m apart; this proximity constitutes a first-order benefit to
412 compare the pace of two different seeps, independently of weather conditions (Fig. 8 A, B). Most
413 of the time, sites A and B were both active, as seepage slicks were identified at both sites for 13
414 scenes out of 20 (Fig. 8 C).

415 We also identified asynchronous active phases from the recognition of isolated seepage slicks on
416 4 images at macro-seep A, while macro-seep B was dormant (pinpointed with black arrows in Fig.

417 8). Based on previous works showing that oil slicks are best detected for wind speeds less than 6-
418 7 m/s (Bern et al., 1992; Espedal and Wahl, 1999), the maximum wind value of 6.5 m/s at these
419 specific sites during short-term monitoring cannot be considered as the factor controlling the
420 absence of seepage (Fig. 8D). In addition, the fact that oil slicks are observed for higher wind
421 speeds during the monitoring period implies that weather conditions were suitable for slick
422 detection. To summarise, all the conditions were satisfied during the three common and
423 asynchronous cessation events for an optimal detection of oil slicks.

424 Furthermore, based on the fact that the disappearance of the seepage slicks is observed between
425 two consecutive SAR acquisitions implies that oil dispersion is effective in less than 12 hours.
426 The reappearance of oil slicks on the following image also indicates that cessation of oil release
427 can occur under restricted time scales.



428

429 **Fig. 8.** A, B. Compilation of oil slick footprints and associated OSOs revealed from short-term
 430 monitoring for macro-seep sites A and B. Colour scale refers to subsequent acquisition dates and
 431 is applied for both seepage slicks and OSOs. Blue circles are the deflection offset computed from
 432 individual OSO locations. C. Red and blue graphs display the length of individual seepage slicks
 433 for seep site A and B respectively. D. Graph of the local wind values derived from SAR scenes.

434 Non-imaged areas were masked with grey squares. Black arrows pinpoint SAR scenes where
435 seepage slicks were only visible from one of the two sites A and B.

436 **4.2.4. *Transience and persistence at micro-seepage sites***

437 A micro-seepage is defined here as a seeping spot with an occurrence rate below 50%. A large
438 number of micro-seepage sites (~1/3) are only associated with a single active event that occurred
439 during the acquisition of SAR scene No. 21 (see yellow dots in Fig. 5). Isolated slick detection
440 occurred during a period of regional increase in the amount of detected oil, while roughly 60% of
441 seeping sites were active. Wind values varied between 1.2 and 6.1 m/s at the OSO location, which
442 is slightly below observed average weather conditions (Fig. 7). Apart from lower occurrence rates,
443 oil slicks expelled from micro seepage sites are revealed by shorter and narrower slicks, showing
444 that the amount of oil released is weaker (Fig. 7A).

445 Micro-seep E identified from 3 recurrent and diverging slicks appears as a new seepage feature on
446 the compilation map that we confidently ranked as natural slicks (Fig. 5). Prior to short-term
447 monitoring, the area was passive, as the SAR data coverage reaches 40 overlapping scenes
448 between 1994 and 2012 (Fig. 2A), but none revealed the presence of seepage slicks at this
449 location. The slicks are characterised by typical curvilinear shapes that have similar trends to the
450 neighbouring slicks on the images, which comforts our presumptions on the natural origin of
451 expelled slicks. This example corresponds to the minimum period of seepage activity observed
452 during the short-term monitoring, revealing that oil release can be ephemeral and temporally
453 constrained to a few days.

454 **5. Discussion**

455 **5.1. Wind requirements for seepage slick detection**

456 The weather requirements for slick detection have been reported by different authors to be 3 to 10
457 m/s (Espedal and Wahl, 1999; Alpers and Espedal, 2004; Girard-Arduin et al., 2005; Brekke and

458 Sölberg, 2005), 3.5 to 7 m/s (Garcia-Pineda et al., 2009) and 1.5 to 10 m/s (Fingas and Brown,
459 2014). During the short-term monitoring, regional wind values ranged among the most restrictive
460 conditions as reported by Garcia-Pineda et al. (2009). The results from seepage studies in the
461 Lower Congo Basin show that weather requirements are constrained between 1.5 and 6.5 m/s
462 (Fig. 7C). Such differences are presumably associated with seepage slick characteristics such as
463 the slick thickness or the oil type (API gravity) that largely varies between petroleum provinces.
464 The wind is also known to affect seepage slicks by separating heavy and light components of oil
465 slicks and spreading oil at the sea surface (Alpers and Espedal, 2004; Marmorino et al., 2008).
466 SAR scene No. 21 records the greatest number of seepages, where two thirds of the imaged sites
467 were active (Figs. 6 and 8). The SAR acquisition was predated by low weather conditions, with
468 regional wind speed around 4 m/s during the 24 preceding hours (Fig. 6). This suggests that ideal
469 weather requirements for seepage slick detection might call for regional low wind conditions not
470 only during, but also predating the SAR acquisition.

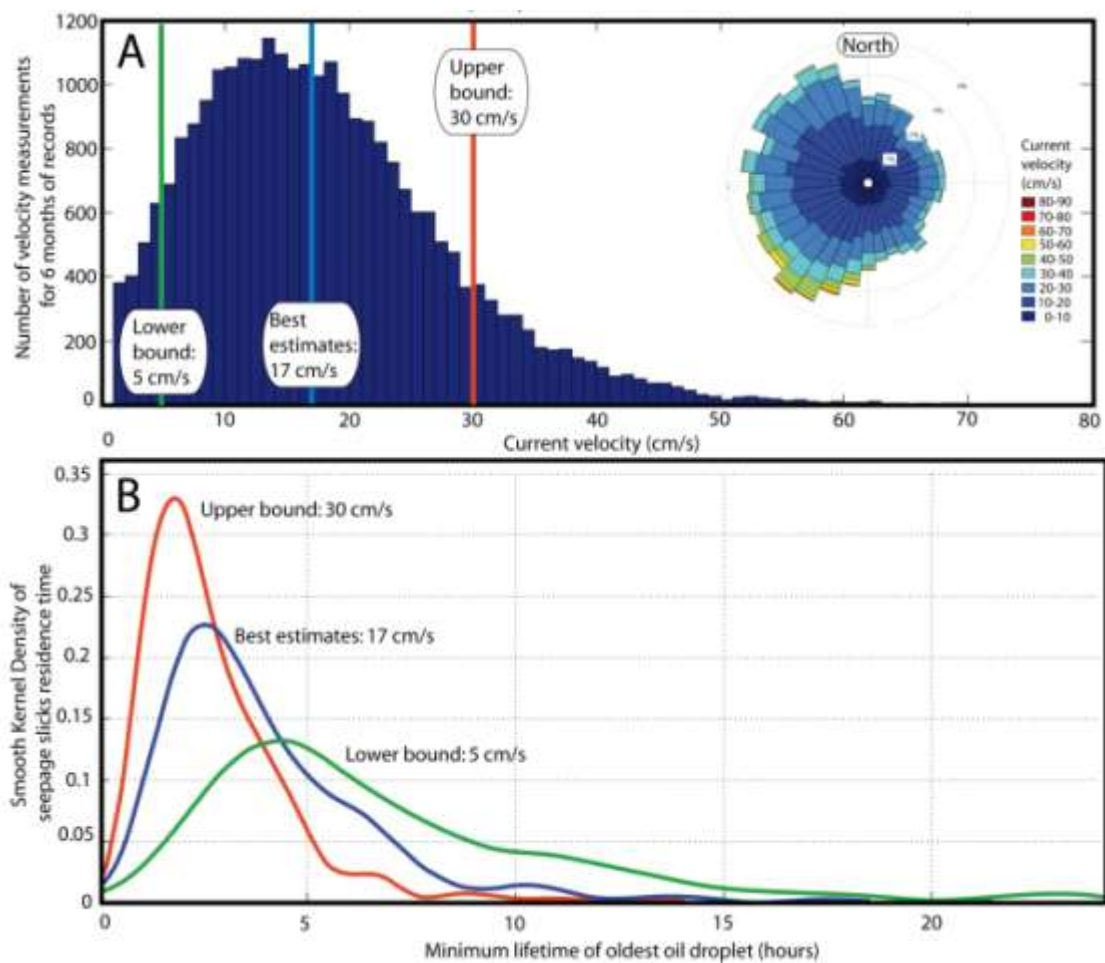
471 **5.2.Seepage slick residence time**

472 Seepage slick residence time was defined from the estimated age of the oil droplet at the distal
473 edge of the slicks (De Beukelear et al., 2003). The restricted length of oil slicks, in addition to
474 brief variations of slick orientation prevent seepage shapes from being fitted between subsequent
475 scenes. This suggests that oil slick dissipation is effective between the acquisitions of two
476 subsequent SAR scenes, typically separated by 12 h.

477 The residence time is approached from the individual slick length divided by the sea surface drift
478 velocity (Macdonald et al., 2015). The velocity of the surface slick displacement is inferred to be
479 induced by 100% of the surface currents in addition to 3% of the wind speed (Kim et al., 2014).
480 The current measurements were not available during short-term monitoring and large scale
481 oceanographic models are unsuitable to characterise local dynamics of the sea surface. We

482 integrated mooring data to characterise the distribution of the surface/subsurface current velocity
483 (Fig. 9A).

484 The mooring data were recorded from January 2009 to July 2009, i.e. three years before short-
485 term monitoring. The integration of ADCP data allowed us to compute a statistical study of the
486 residence time of oil slicks at the sea surface during short-term monitoring using the near surface
487 velocity of the current (10 m below the sea surface) and the local wind from derived SAR scenes.
488 Surface velocity ranged between 0 and 81 cm/s during the 6 months of mooring. Among this
489 range, 85% of measured velocity lies between 5 and 30 cm/s with a median velocity value of 17
490 cm/s. We made three estimations of residence time considering a lower bound for a conservative
491 current velocity of 5 cm/s, an upper bound for an overstating current velocity of 30 cm/s and a
492 best estimate for the median current velocity of 17 cm/s (Fig. 9B).



493

494 **Fig. 9.** A: Histogram of the distribution of current speed recorded from 6 months of mooring
495 measurements 10 m below the sea surface. We considered an upper and a lower bound from the
496 overall distribution of the current velocity. The wind rose to the right shows the distribution of
497 current orientation and speed. B: Smooth kernel density of the distribution of the minimum
498 residence time of the oldest oil droplet of individual slicks mapped during short-term monitoring.
499 The residence time computation considers the local wind value at the location of OSOs, surface
500 current velocity and slick length.

501 The estimation of theoretical residence times shows that their distribution gathers around the
502 median value for the upper, median and lower bound. The distribution progressively decreases
503 from this median value. The median residence time value for the upper bound at 30 cm/s is
504 2h15min, 3h15min for the median value of 17 cm/s and 5 h 30min for the lower bound at 5 cm/s.
505 The slick residence time for median estimates is mostly distributed between 1 and 7 hours.

506 The natural seepage residence time was inferred to be comprised between 8 and 24 h by Mitchell
507 et al. (2000) and MacDonald et al. (2015) for the Gulf of Mexico. Seepage residence time in this
508 study is lower than previously suggested, as best estimates suggest that median residence time is
509 3h15min. The residence times from this study are rather in agreement with Marmorino et al.
510 (2008), who suggested that they concentrate below 5 hours. Restricted residence time has great
511 implication on the hydrocarbon flux and therefore on quantifications of the regional oil output.
512 The short lifetime of seepage slicks can be explained from the relative expelled amount that is
513 probably lower in the Lower Congo Basin than in the Gulf of Mexico, but also by severe
514 weathering conditions along warm Angolan coasts (Hardman-Mountford et al., 2003) that largely
515 contribute to spill dispersion (Leifer et al., 2012).

516 However, these observations refer to short-term monitoring, where the length of the oil slicks
517 varies between 1000 and 17,000 m (Fig. 7), yet seepage slicks were mapped with greater lengths
518 during long-term monitoring (Fig. 3A and B). Observations of slicks greater than 30 km long

519 remained unusual (less than 1% of slick collection) but suggest that slick residence time can
520 occasionally be greater than values computed from short-term monitoring. Such exceptional
521 observations of lengthened slicks could also be explained by a substantial increase in surface
522 displacement velocity or predated by consistent low wind conditions before SAR acquisition.

523 **5.3. Evidence of leakage interruption**

524 The non-detection of seepage slicks on SAR scenes can either be explained by unsuitable wind
525 conditions or as an evidence of a consistent decrease of the amount of expelled oil that prevents
526 the detection of slicks by the SAR system. The comparison between the distributions of local
527 wind values at recurrent seep sites between active and dormant stages remained concordant (Fig.
528 7). The wind distribution at the location of recurrent sites during dormant periods were imaged
529 during the ideal weather conditions (Fig. 7D) which demonstrates that the non-detection of
530 seepage slicks is associated with a short-term intermittence.

531 It was established in the Black Sea (Greinert et al., 2006) and Gulf of Mexico (Garcia-Pineda et
532 al., 2010) that gas seepage rates from cold seeps may be highly variable over time. Leifer et al.,
533 (2004) and Garcia-Pineda et al. (2016) also demonstrated this variability for oil seepage in the
534 Santa Barbara basin and the Gulf of Mexico, respectively.

535 Concordant observations performed from long-term and short-term monitoring suggesting that oil
536 seepage is also discontinuous in the Lower Congo Basin are listed below:

537 - The great variability of occurrence rates values ranging from 5 to 80% shows that the amount of
538 released oil significantly differs between seeping sites, suggesting recurrent interruption of oil
539 release with varying frequencies between seep sites.

540 - Recurrent twin slicks were identified at the location of the two macro-seep sites A and B, which
541 are separated by a distance of 2250 m. The identification of concordant shapes for neighbouring
542 slicks on SAR data (Figs. 3 and 8) proves that they are expelled simultaneously from distinct

543 sources (MacDonald et al., 1993; Garcia-Pineda et al., 2010; Körber et al., 2014). Therefore, the
544 identification of a single seep suggests the leakage interruption of one of the two sites instead of
545 unsuitable meteorological conditions (Fig. 8).

546 - Seep site E (see location in Fig. 6) was characterised by a restricted active period of a few hours.
547 The observations of recurrent slicks over a restricted period can be either explained as associated
548 with ephemeral seep sites or with a consistent increase in the amount of expelled oil.

549 - The seep triplets in the northernmost area (Fig. 6) lie in the underwater investigation area studied
550 by Wenau et al. (2014). The detection of acoustic anomalies is commonly used to identify seepage
551 bubble trains in the water column (De Beukelear et al., 2003; Körber et al., 2014). The area was
552 considered as inactive, as the water column records did not reveal any typical acoustic anomaly at
553 this location. This demonstrates that the three oil seeps were dormant during the few days of
554 underwater investigations and further supports the hypothesis of intermittent seepage activity.

555 The integration of SAR data characterised by a swath several hundred of kilometres wide provides
556 an interesting means to monitor several oil seeps simultaneously. Mesoscale events, such as
557 seismic events (Zatyagalova et al., 2007) or hydrostatic variation of pressure (Boles, 2001; Glasby
558 et al., 2001; Chanton et al., 2003; Rollet et al., 2006) were demonstrated to be associated to a
559 variation of the amount of expelled fluids. Conversely, our results regarding the regional seepage
560 pace indicate that individual seep sites can have their own periodicity (see examples of seep sites
561 A and B) with miscellaneous active and inactive stages.

562 **5.4. Insights on seepage pace from short- and long-term monitoring**

563 The short-term pace of seepage activity appears highly variable. The maximum duration of
564 seepage activity was observed for Seep A, where slicks were detected on six consecutive scenes
565 showing that they remained active during at least 3 days. In addition, inactive periods of macro-
566 seep sites are restricted to daily periods (Fig. 9), revealing that the seeping mechanism may be
567 transient at a daily scale. The recurrent lack of seepage slick detection above macro-seepage sites

568 suggests at least a great decrease of both the volume of expelled oil and the slick thickness
569 preventing the slick detection from SAR scenes detectability threshold.

570 Among the 102 seep sites (Fig. 4), 48 minor seep sites (occurrence rate lower than 30%) were
571 passive during the short-term monitoring acquisitions (black stars in Fig. 5), revealing that
572 inactive stages can be longer than 10 days. Occurrence rates of macro-seep sites are consistent
573 between short-term monitoring and long-term monitoring. This suggests that the relative macro-
574 seep activity observed over the short-term period remain constant over decades.

575 In addition, non-recurrent slicks were observed from 140 seepage slicks (10%) during long-term
576 monitoring (isolated white dots in Fig. 4A). Assuming that the acquisition frequency of SAR
577 scene acquisitions was low between 1994 and 2012 (4 to 5 scenes each year in average), non-
578 recurrent slicks detected during the long-term monitoring are presumably associated with
579 ephemeral expulsions sites, as demonstrated by the short-term monitoring (seep site E). The high
580 variability of the amount of expelled oil suggests that the evaluation of the seepage activity during
581 scientific exploration campaigns should be based on a consistent period of underwater records.

582 **5.5. Oil output quantification**

583 From oceanographic investigations and SAR observations, the minimum detectable thickness for
584 oil film can be estimated at 0.1 μm (Allen, 1970; Macdonald et al., 1993; Mitchell, 2000;
585 Macdonald et al., 2002; Garcia-Pineda et al., 2009). From the Bonn agreements (2009), which
586 established a relationship between the visual aspect of oil slicks and their thickness in the offshore
587 domain, Garcia-Pineda et al. (2013) considered that the thickness of an oil slick is 1 μm for 5% of
588 the fresher slick surface and 0.1 μm for the remaining 95% of the surface. Based on this
589 assumption, a slick of 1 km^2 may therefore contain 145 l of oil. Considering this thickness, the
590 sum of oil-covered surface within each grid cells gives a total average amount of 1625 litres at the
591 sea surface (Fig. 5). Considering a median residence time at the sea surface computed with the
592 subsurface current (Fig. 9) and the local wind velocity (Fig. 7), we performed a volumetric

593 computation of regional oil output for the 102 natural seeps along the Angolan coasts (Table 4).
 594 The median estimate, considered as the best estimate and computed using an average surface
 595 current velocity (Fig 9), indicates that 500 litres are expelled each hour, which represents an
 596 annual amount of 4380 m³ of oil naturally expelled in the Lower Congo Basin.

597 **Table 4**

598 Estimation of the regional output of oil from the 102 natural seeps along the Lower Congo Basin,
 599 assessed from average surface oil and SAR data coverage.

Average surface oil volume (l)	Lower Bound	Median estimate	Upper bound
Considered subsurface current velocity (cm/s)	5	17	30
Median residence time	5h30min	3h15min	2h15min
Average output (l/h)	295.45	500	722.22
Annual amount (l/yr)	2.58*10 ⁶	4.38*10 ⁶	6.32*10 ⁶
Annual amount (bbl/yr)	1.62*10 ⁴	2.75*10 ⁴	3.97*10 ⁴

600
 601 To give a comparison, Macdonald et al. (2015) assessed the annual output across the entire Gulf
 602 of Mexico as between 25,300 m³ and 94,800 m³ per year. Hornafius et al. (1999) estimated oil
 603 seepage along the Santa Barbara basins around 5840 m³. For the southwestern Caspian Sea,
 604 Zatygalova et al. (2007) evaluated a minimum natural seepage rate of 1700 m³. Estimations
 605 performed by Körber et al. (2014) suggest that about 360 m³ are expelled for the eastern Black
 606 Sea. The most accurate estimation presented in this paper therefore rank the Lower Congo Basin
 607 as the third biggest oil-supplying area in the world. The computations of expelled volumes based
 608 on the gridded method developed by Macdonald et al. (2015) are detached from the dimensions of
 609 the study areas. The orders of magnitude of the surface oil volume are comparable between the
 610 Gulf of Mexico (<15 l/km²) and the Lower Congo Basin (<10 l/km²), where oil seep systems are
 611 related to salt tectonics in both cases. The seepage intensity per unit area should be compared for
 612 miscellaneous geological contexts to understand bypass system efficiency. Thermogenic seep

613 sites are also associated with a consistent methane flux (Solomon et al., 2009; Hu et al., 2012),
614 benefiting from both thermal cracking and biodegradation (Head et al., 2003; Peters and
615 Moldowan, 2007). Even if the gas quantification associated with oil escapes remains an open
616 question, this amount is presumably considerable. The assessment of contemporary seepage
617 volumes also provides calibration tips for the evaluation of fossil seep systems. Ongoing work
618 integrating the SAR dataset together with subsurface geophysical imagery will help to associate
619 sea surface evidences of oil leakage with seafloor venting features.

620 **Conclusions**

621 This study integrates a combination of long-term (82 images over 18 years) and short-term (22
622 images over 10 days) monitoring of SAR scenes to understand the seepage situation in the Lower
623 Congo Basin. The compilation map of recurrent seepage slicks forms diverging oil slick patterns
624 from the central origin area, which allowed the recognition of 102 recurrent oil seeping sites. The
625 seeping area is constrained to the compressive and translated salt-related structural domains,
626 where salt diapirs create efficient oil migration pathways to the sea surface. It was demonstrated
627 that the occurrence rates strongly vary between seeping sites, ranging from 5 to 80%. The
628 correlation of SAR observations with wind speeds showed that slick detection is possible for wind
629 values ranging from 1.5 to 6.5 m/s. Local winds at dormant sites remain within ideal weather
630 conditions demonstrating the intermittent activity and the high variability of seepage flow rates
631 over short periods. This allowed the identification of macro-seep sites of high occurrence rates
632 and micro-seepage sites releasing hydrocarbons sparsely or ephemerally towards the sea surface.
633 Merely half of the seeping sites revealed from 18-year long-term monitoring were active during
634 10-day short-term monitoring, suggesting that the remaining half remained dormant. Short-term
635 monitoring shows that the slick residence time is low, as the seepage signal is lost between two
636 consecutive SAR scenes separated by 12 h. Sea surface speed displacement estimated from the
637 integration of local winds and subsurface current measurements, coupled with slick lengths

638 allowed us to provide for the first time a statistical study and a quantitative approach to assess the
639 surface slick residence time. This distribution concentrates around a median value of 3h15min.
640 The best estimates of the volumetric outflow give an annual volume of 4380 m³ of oil naturally
641 expelled in the Lower Congo Basin.

642 **Acknowledgements**

643 The authors would like to express their grateful thanks to Marc Lucas and Nicolas Long  p   from
644 CLS (Collecte Localisation Satellites) for their constructive contributions with satellite data
645 tasking and processing for wind field data computation. This study has been performed as a part
646 of a PhD project in the framework of a CIFRE contract funded by Total SA and granted by the
647 ANRT (Agence National de la Recherche et de la Technologie). The project built on a
648 collaboration with the University of Perpignan, France. The satellite data were provided by the
649 European Space Agency (Envisat WSM, IMP), Canadian Space Agency (Radarsat), German
650 Aerospace Centre (Terrasar-X) and Italian Space Agency (Cosmo-skymmed). We deeply thank
651 two anonymous reviewers and Pr. I. MacDonald for their critical comments and suggestions that
652 improved the content of the paper.

653 **References**

- 654 Arhan, M., Mercier, H., Park, Y.H. (2003), On the deep water circulation of the eastern South
655 Atlantic Ocean. *Deep Sea Research Part I: Oceanographic Research Papers*, 50(7), 889-916.
- 656 Allen, A.A., Schlueter, R.S., Mikolaj, P.G. (1970), Natural oil Seepage at Coal Oil Point, Santa
657 Barbara, California. *Science*, 170, 974 – 977.
- 658 Alpers, W., & Espedal, H.A. (2004), Oils and Surfactants in *SAR Marine User's Manual*.
- 659 Andresen, K.J., Huuse, M., Sh  dt., N.H., Clausen, F., Seidler, L. (2010), Hydrocarbon plumbing
660 systems of salt minibasins offshore Angola revealed by three-dimensional seismic analysis, *AAPG*
661 *Bulletin*, 95, 1039-1065, <http://dx.doi.org/10.1306/12131010046>.

662 Andresen K.J., Huuse, M. (2011), 'Bulls-eye' and polygonal faulting in the Lower Congo Basin:
663 Relative timing and implications for fluid expulsion during shallow burial, *Marine Geology*, 279,
664 111-127, <http://dx.doi.org/10.1016/j.margeo.2010.10.016>.

665 Andresen, K.J. (2012), Fluid flow features in hydrocarbon plumbing systems: What do they tell us
666 about the basin evolution, *Marine Geology*, 332-334, 89-108,
667 <http://dx.doi.org/10.1016/j.margeo.2012.07.006>.

668 Anka, Z., Séranne, M., Lopez, M., Scheck-Wenderoth, M., Savoye, B. (2009), The long-term
669 evolution of the Congo deep-sea fan: A basin-wide view of the interaction between a giant
670 submarine fan and a mature passive margin (ZaiAngo project), *Tectonophysics* 470, 42-56,
671 <http://dx.doi.org/10.1016/j.tecto.2008.04.009>.

672 Anka, Z., Ondrak, R., Kowitz, A., Schodt, N. (2013), Identification and numerical modeling of
673 hydrocarbon leakage in the Lower Congo Basin: Implications on the genesis of km-wide seafloor
674 mounded structures, *Tectonophysics*, 604, 153-171, <http://dx.doi.org/10.1016/j.tecto.2012.11.020>.

675 Beglinger, S.E., Doust, H., Cloetingh, S. (2012), Relating petroleum system and play
676 development to basin evolution: West African South Atlantic basins, *Marine and Petroleum*
677 *Geology*, 30, 1-25, <http://dx.doi.org/10.1016/j.marpetgeo.2011.08.008>.

678 Bern, T.I., Wahl, T., Anderssen, T., Olsen, R. (1992), Oil Spill detection using satellite based
679 SAR: experience from a field Experiment, *Proceedings First ERS-1 Symposium - Space at the*
680 *Service of our Environment*, 829 – 834.

681 Boyer, D., Cole, J., Bartholomae, C. (2000), Southwestern Africa: Northern Benguela Current
682 Region, *Marine Pollution Bulletin*, 41, 123-140.

683 Brekke, C., Solberg, A.H.S. (2005), Oil spill detection by satellite remote sensing, *Remote*
684 *Sensing of Environment*, 95, 1-13, <http://dx.doi.org/10.1016/j.rse.2004.11.015>.

685 Brice, S.E., Cochran, M.D., Pardo, G., Edwards, A.D. (1982), Tectonics and sedimentation of the
686 South Atlantic Rift Sequence: Cabinda, Angola. *American Association Petroleum Geologists*
687 *Memoir*, 34, 5– 18.

688 Brownfield, M.E., & Charpentier, R.R. (2006), Geology and total petroleum systems of the west-
689 central coastal province (7203), west Africa (No. 2207-B).

690 Brun, J.P., Fort, X. (2004), Compressional salt tectonics (Angolan Margin), *Tectonophysics*, 382,
691 129– 150, <http://dx.doi.org/10.1016/j.tecto.2003.11.014>.

692 Burwood, R., (1999), Angola: source rock control for Lower Congo Coastal and Kwanza Basin
693 petroleum systems, *Geological Society*, London, Special Publications v. 152, p181-184.

694 Cainelli, C., Mohriak, W.U. (1999), Some remarks on the evolution of sedimentary basins along
695 the eastern Brazilian continental margin, *Episodes*, 22:3, 206-216.

696 Charlou, J.L., Donval, J.P., Fouquet, Y., Ondreas, H., Knoery, J., Cochonat, P., Levaché, D.,
697 Poirier, Y., Jean-Baptiste, P., Fourré, E., Chazallon, B. (2004), Physical and chemical
698 characterization of gas hydrates and associated methane plumes in the Congo–Angola Basin
699 *Chemical Geology*, 205, 405 – 425, <http://dx.doi.org/10.1016/j.chemgeo.2003.12.033>.

700 Chen, S., & Hu, C. (2014), In search of oil seeps in the Cariaco basin using MODIS and MERIS
701 medium-resolution data. *Remote Sensing Letters*, 5(5), 442-450.

702 Da Costa, J.L., Schirmer, T.W., Laws, B.R. (2000), Lower Congo basin, Deepwater Exploration
703 Province, Offshore West Africa, *Second Wallace E. Pratt memorial Conference 3 Petroleum*
704 *Provinces of the 21st Century*.

705 De Beukelear, S.M., MacDonald, I.R., Guinasso, N.L., Murray, J.A. (2003), Distinct side-scan
706 sonar, RADARSAT SAR, and acoustic profiler signatures of gas and oil seeps on the Gulf of
707 Mexico slope, *Geo-Marine Letters*, 23, 177-186.

708 Deffontaines, B., Riazanoff, S., Najoui, Z., Facon, M., (2014), Monitoring marine oil seeps from
709 space : the African Case. *The 13th HGS-PESGB Conference on African E&P*

710 Dhont, D., Cauquil, E., Jatiault, R., 2013, Relation between Oil Seeps and Seabed Morphologies,
711 *Offshore technology Conference paper n°24242.*

712 Doi, T., Tozuka, T., Sasaki, H., Masumoto, Y., Yamagata, T. (2007), Seasonal and interannual
713 variations of oceanic conditions in the Angola Dome. *Journal of Physical Oceanography*, 37(11),
714 2698-2713.

715 Duval, B., Cramez, C., Jackson, M.P.A. (1991), Raft tectonics in the Kwanza Basin, Angola,
716 *Marine and Petroleum Geology*, 9, 389 – 404.

717 Espedal, H.A., Johannessen, O.M. (2000), Detection of oil spills near offshore installations using
718 synthetic aperture radar (SAR), *International Journal of Remote Sensing*, 21:11, 2141-2144,
719 <http://dx.doi.org/10.1080/01431160050029468>.

720 Espedal, H.A., Wahl, T. (1999), Satellite SAR oil spill detection using wind history information,
721 *International Journal of Remote Sensing*, vol. 20, 49-65.

722 Etiope, G. (2015), Natural Gas Seepage – The Earth’s Hydrocarbon Degassing.

723 Fingas, M., & Brown, C. (2014), Review of oil spill remote sensing. *Marine pollution bulletin*,
724 83(1), 9-23. <http://dx.doi.org/10.1016/j.marpolbul.2014.03.059>.

725 Franceschetti, G., Iodice, A., Riccio, D., Ruello, G. Siviero, R. (2002), SAR Raw Signal
726 Simulation of Oil Slicks in Ocean Environments, *IEEE transactions on geosciences and remote*
727 *sensing*, 40:, 1935 – 1949.

728 Fort, X., Brun, J.P., Chauvel, F. (2004), Salt tectonics on the Angolan margin, synsedimentary
729 deformation processes, *AAPG Bulletin*, 88:11, 1523–1544.

730 Gade, M., Alpers, W. (1998), Imaging of biogenic and anthropogenic ocean surface films by the
731 multifrequency/ multipolarization SIR-C/X-SAR, *Journal of Geophysical Research*, 103, 18851-
732 18866.

733 Garcia-Pineda, O., Zimmer, B., Howard, M., Pichel, P., Li, X., MacDonald, I.R. (2009), Using
734 SAR images to delineate ocean oil slicks with a texture-classifying neural network algorithm
735 (TCNNA), *Canadian journal of Remote Sensing*, 35, 411-421.

736 Garcia-Pineda, O., MacDonald, I., Zimmer, B., Shedd, B., Roberts, H., (2010), Remote-sensing
737 evaluation of geophysical anomaly sites in the outer continental slope, northern Gulf of Mexico,
738 *Deep-Sea research II* 57, 1859-1869, <http://dx.doi.org/10.1016/j.dsr2.2010.05.005>.

739 Garcia-Pineda, O., MacDonald, I., Shedd, W. (2013), Analysis of oil fluxes of hydrocarbon seep
740 formations on the Green Canyon and Mississippi Canyon: a study using 3-d seismic attributes in
741 combination with satellite and acoustic data, *Offshore Technology Conference 24226*.

742 Garcia-Pineda, O., MacDonald, I., Shedd, W. (2014), Analysis of oil-volume fluxes of
743 hydrocarbon-seep formations on the Green canyon and Mississippi canyon: A study with 3D
744 Seismic Attributes in combination with satellite and acoustic data, *SPE Reservoirs Evaluation and*
745 *Engineering*.

746 Garcia-Pineda, O., MacDonald, I., Silva, M., Shedd, W., Asl, S. D., Schumaker, B. (2016),
747 Transience and persistence of natural hydrocarbon seepage in Mississippi canyon, Gulf of
748 Mexico. *Deep Sea Research Part II: Topical Studies in Oceanography*, 129, 119-129.

749 Gay, A., Lopez, M., Cochonat, P., Sultan, N., Cauquil, E., Brigaud, F. (2003), Sinuous pockmark
750 belt as indicator of a shallow buried turbiditic channel on the lower slope of the Congo Basin,
751 West African Margin. In: Van Rensbergen, P., Hillis, R.R., Maltman, A.J., Morley, C.K.,
752 *Subsurface Sediment Mobilization, Geological Society of London, Special Publications, vol. 216*,
753 173–189.

754 Gay, A., Lopez, M., Berndt, C., Séranne, M. (2007), Geological controls on focused fluid flow
755 associated with seafloor seeps in the Lower Congo Basin, *Marine Geology* 244, 68 – 92,
756 <http://dx.doi.org/10.1016/j.margeo.2007.06.003>.

757 Gay, A., Lopez, M., Cochonat, P., Levaché, D., Sermondadaz, G., Seranne, M. (2006 a),
758 Evidences of early to late fluid migration from an upper Miocene turbiditic channel revealed by 3D
759 seismic coupled to geochemical sampling within seafloor pockmarks, Lower Congo Basin,
760 *Marine and Petroleum geology* 23, 387-399, <http://dx.doi.org/10.1016/j.marpetgeo.2006.02.004>.

761 Gay, A., Lopez, M., Cochonat, P., Séranne, M., Levaché, D., Sermondadaz, G. (2006 b), Isolated
762 seafloor pockmarks linked to BSRs, fluid chimneys, polygonal faults and stacked Oligocene–
763 Miocene turbiditic paleochannels in the Lower Congo Basin, *Marine Geology* 226, 25 – 40,
764 <http://dx.doi.org/10.1016/j.margeo.2005.09.018>.

765 Gay, A., Lopez, M., Ondreas, H., Charlou, J.L., Sermondadaz, G., Cochonat, P. (2006 c), Seafloor
766 facies related to upward methane flux within a Giant Pockmark of the Lower Congo basin, *Marine*
767 *Geology* 226, 81 – 95, <http://dx.doi.org/10.1016/j.margeo.2005.09.011>.

768 Girard-Ardhuin, F., Mercier, G., Collard, F., Garello, R. (2005), Operational Oil-Slick
769 Characterization by SAR Imagery and Synergistic Data, *IEEE Journal of Oceanic Engineering*,
770 30:3, 487 – 495.

771 Gordon, R. L., & Instruments, R. D. (1996), Principles of operation a practical primer. *RD*
772 *Instruments, San Diego*.

773 Greinert, J., Artemov, Y., Egorov, V., De Batist, M., McGinnis, D. (2006), 1300-m-high rising
774 bubbles from mud volcanoes at 2080m in the Black Sea: Hydroacoustic characteristics and
775 temporal variability, *Earth and Planetary Science Letters*, 244, 1–15,
776 <http://dx.doi.org/10.1016/j.epsl.2006.02.011>.

777 Guilbot, J., Cagnol, J.L., Stankoff, M., Bouroullec, J.L., Lemasitre, L. (2010), Subsalt
778 Exploration, Appraisal and Development Challenges in Gulf of Guinea: Example of Block 32 -
779 Angola.

780 Hardman-Mountford, N.J., Richardson, A.J., Agenbag, J.J., Hagen, E., Nykjaer, L., Shillington,
781 F.A., Villacastin, C. (2003), Ocean climate of the South East Atlantic observed from satellite data
782 and wind models, *Progress in Oceanography*, 59, 181-221,
783 <http://dx.doi.org/10.1016/j.pocean.2003.10.001>.

784 Head, I. M., Jones, D.M., Larter, S.R. (2003), Biological activity in the deep subsurface and the
785 origin of heavy oil. *Nature*, 426(6964), 344-352.

786 Holmes, M.E., Schneider, R.R., Müller, P.J. (1997), Reconstruction of past nutrient utilization in
787 the eastern Angola Basin based on sedimentary $^{15}\text{N}/^{14}\text{N}$ ratio 1997, *Paleoceanography*, 12:4,
788 604-614.

789 Hopkins, J., Lucas, M., Dufau, C., Sutton, M., Stum, J. (2013), Detection and variability of the
790 Congo River plume from satellite derived sea surface temperature, salinity, ocean colour and sea
791 level. *Remote Sensing of Environment*, 139, 365-385.

792 Hornafius, J. S., Quigley, D., Luyendyk, B.P. (1999), The world's most spectacular marine
793 hydrocarbon seeps (Coal Oil Point, Santa Barbara Channel, California): Quantification of
794 emissions. *Journal of Geophysical Research: Oceans*, 104(C9), 20703-20711.

795 Hu, C., Li, X., Pichel, W.G., Muller-Karger, F.E. (2009), Detection of natural slicks in the NW
796 Gulf of Mexico using MODIS imagery, *Geophysical Research Letters*, 36,
797 <http://dx.doi.org/10.1029/2008GL036119>.

798 Hu, L., Yvon-Lewis, S.A., Kessler, J.D., MacDonald, I.R. (2012), Methane fluxes to the
799 atmosphere from deepwater hydrocarbon seeps in the northern Gulf of Mexico. *Journal of*
800 *Geophysical Research: Oceans*, 117(C1).

801 Ivanov, A.Y., Gobulov, B.N., Zatyagalova, B.B. (2007), On oil and gas seeps and underground
802 fluid discharges in the Southern Caspian based on Space Radar Data, *Earth Exploration from*
803 *Space*, 2, 62-81.

804 Johannessen, O.M., Sandven, M., Jenkins, A.D., Durand, D., Petterson, L.H., Espedal, H.,
805 Evensen, G., Hamre, T. (2000), Satellite earth observation in operational oceanography, *Coastal*
806 *Engineering*, 41, 155-176.

807 Jackson, C.R., da Silva, J.C., Jeans, G., Alpers, W., Caruso, M.J. (2013), Nonlinear internal waves
808 in synthetic aperture radar imagery. *Oceanography*, 26(2), 68-79, [http://dx.doi.org/10.5670/](http://dx.doi.org/10.5670/oceanog.2013.32)
809 [oceanog.2013.32](http://dx.doi.org/10.5670/oceanog.2013.32).

810 Jones, D.O.B., Walls, A., Clare, M., Fiske, M.S., Weiland, R.J., O'Brien, R., Touzel, D.F. (2014),
811 Asphalt mounds and associated biota on the Angolan margin, *Deep-Sea Research I*,
812 <http://dx.doi.org/10.1016/j.dsr.2014.08.010>.

813 Kim, T.H., Yang, C.S., Oh, J.H., Ouchi, K. (2014), Analysis of the Contribution of Wind drift
814 factor to oil slick Movement under strong tidal condition. Hebei Spirit Oil Spill Case. *Plos ONE*,
815 9(1), e87393.

816 King, L.H., & MacLean, B. (1970), Pockmark on the Scotian Shelf, *Geological Society of*
817 *America Bulletin*, V.81, P.3141-3148.

818 Körber, J.H., Sahling, H., Pape, T., dos Santos Ferreira, C., MacDonald, I., Bohrmann, G. (2014),
819 Natural oil seepage at Kobuleti Ridge, eastern Black Sea. *Marine and Petroleum Geology*, 50, 68-
820 82, <http://dx.doi.org/10.1016/j.marpetgeo.2013.11.007>.

821 Kornacki, A.S., Kendrick, J.W., Berry, J.L. (1994), Impact of oil and gas vents and slicks on
822 petroleum exploration in the deepwater Gulf of Mexico, *Geo-Marine Letters*, 14, 160-169.

823 Kvenvolden, K.A., Cooper C.K. (2003), Natural seepage of crude oil into the marine
824 environment, *Geo-Marine Letters*, 23, 140-146, <http://dx.doi.org/10.1007/s00367-003-0135-0>.

825 Kvenvolden, K. A., & Rogers, B.W. (2005), Gaia's breath—global methane exhalations. *Marine*
826 *and Petroleum Geology*, 22(4), 579-590.

827 Lass, H.U., Schmidt, M., Mohrholz, V., Nausch, G. (2000), Hydrographic and Current
828 Measurements in the Area of the Angola–Benguela Front, *Journal of Physical Oceanography*, 30,
829 2589 – 2609.

830 Leifer, I., Boles, J.R., Luyendyk, B.P., Clark, J.F. (2004), Transient discharges from marine
831 hydrocarbon seeps: spatial and temporal variability, *Environmental Geology*, 46, 1038-1052,
832 <http://dx.doi.org/10.1007/s00254-004-1091-3>.

833 Lynn., R.J. (1971), On Potential Density in the Deep South Atlantic Ocean, *Journal of Marine*
834 *research*, 29, 171 – 177.

835 MacDonald, I.R., Garcia-Pineda, O., Beet, A., Daneshgar Asl, S., Feng, L., Graettinger, G.,
836 French-McCay, D., Holmes, J., Hu, C., Huffer, F., Leifer, I., Muller-Karger, F., Solow, A., Silva,
837 M., Swayze, G. (2015), Natural and unnatural oil slicks in the Gulf of Mexico. *Journal of*
838 *Geophysical Research: Oceans*, 120(12), 8364-8380.

839 Macdonald, I.R., Guinasso, N.L., Ackleson, S.G., Amos, J.F., Duckworth, R., Sassen, R. (1993),
840 Natural oil slicks in the gulf of Mexico visible from space, *Journal of Geophysical Research*, 98,
841 16351 – 16364.

842 Macdonald, I.R., Leifer, I., Sassen, R., Stine, P., Mitchell, R., Guinasso, J.N. (2002), Transfer of
843 hydrocarbons from natural seeps to the water column and atmosphere. *Geofluids*, 2, 95-107.

844 MacDonald, I.R., Reilly, J.F. Jr., Best, S.E., Venkataramaiah, R., Sassen, R., Guinasso, N.L. Jr.,
845 Amos, J. (1996), Remote sensing inventory of active oil seeps and chemosynthetic communities

846 in the northern Gulf of Mexico, in D. Schumacher and M. A. Abrams, eds., Hydrocarbon
847 migration and its near-surface expression: *AAPG Memoir*, 66, 27–37.

848 Marmorino, G.O., Smith, G.B., Toporkov, J.V., Sletten, M.A., Perkovic, D., Frasier S.J. (2008),
849 Evolution of ocean slicks under a rising wind, *Journal of Geophysical research*, 113, 1 – 13,
850 <http://dx.doi.org/10.1029/2007JC004538>.

851 Marton, G., Carpenter, D., Greg, S. (2004), Salt Tectonics of the Continent-Ocean Transition,
852 Deep-Water Angola: Concepts, Applications and Case Studies for the 21st Century, *24th Annual*
853 *GCSSEPM Foundation Bob F. Perkins Research Conference*.

854 McCandless, S.W., & Jackson, C.R. (2003), Principles of Synthetic Aperture Radar in *Synthetic*
855 *Aperture Radar Marine User's Manual*, 1-24.

856 Mitchell, R., MacDonald, I.R., Kvenvolden, K.K. (2000), Estimates of total hydrocarbon seepage
857 into the Gulf of Mexico based on satellite remote sensing images. In: *Conf Proc 2000 Ocean*
858 *Sciences Meet 1999, San Antonio, Texas. Am. Geophys Union, vol. OS411-02*.

859 Moroshkin, K.V., Bunov, V.A., Bulatov, R.P. (1970), Water circulation in the eastern South
860 Atlantic Ocean. *Oceanology*, 10, 27–34.

861 National Research Council Committee on Oil in the Sea (2003), Oil in the Sea III: Inputs, Fates
862 and Effects, 280 pp., The National Academies Press, Washington, D. C.

863 Ondreas, H., Olu, K., Fouquet, Y., Charlou, J.L., Gay, A., Dennielou, B., Donval, J.P., Fifis, A.,
864 Nadalig, T., Cochonat, P., Cauquil, E., Bourillet, J.F., Le Moigne, M., Sibuet, M. (2005), ROV
865 study of a giant pockmark on the Gabon continental margin, *Geo-Marine Letters*, 25, 281-292,
866 <http://dx.doi.org/10.1007/s00367-005-0213-6>.

867 Peters, K.E., Walters, C.C., Moldowan, J.M. (2007), The Biomarker Guide Volume 2, Biomarkers
868 and Isotopes in Petroleum Systems and Earth History.

869 Peterson, R.G., Stramma, L. (1991), Upper-level circulation in the South Atlantic Ocean,
870 *Progress in Oceanography*, 26, 1-73.

871 Rowe, F., & Young, J. (1979), An ocean current profiler using Doppler sonar, Oceans '79
872 Proceedings.

873 Sahling, H., Bohrmann, G., Spiess, V., Bialas, J., Breitzke, M., Ivaniov, I., Kasten, S., Krastel, S.,
874 Schneider, R. (2008), Pockmarks in the Northern Congo Fan area, SW Africa: Complex seafloor
875 features shaped by fluid flow, *Marine Geology*, 249, 206-225,
876 <http://dx.doi.org/10.1016/j.margeo.2007.11.010>.

877 Schneider, R.R., Müller, P.J., Ruhland, G., Meinecke, G., Schmidt, H., Wefer, G. (1996), Late
878 Quaternary Surface Temperatures and Productivity in the East-Equatorial South Atlantic:
879 Response to Changes in Trade/ Monsoon Wind Forcing and Surface Water Advection in Wefer,
880 G., Berger, W.H., Siedler, G., Webb, O.J., 1996, *The South Atlantic: Present and Past*
881 *Circulation*, 527 – 551.

882 Schoellkopf, N.B., Patterson, B.A. (2000), Petroleum systems of offshore, Cabinda, Angola, in M.
883 R. Mello and B. J. Katz, Petroleum systems of South Atlantic margins: *AAPG Memoir 73*, 361–
884 376.

885 Shannon, L.V. (2001), Benguela Current, in *Ocean Currents: a derivative of encyclopedia of*
886 *Ocean Sciences*, 2nd Edition, p. 23-34.

887 Skrunes S. (2014), Characterization of Low backscatter Regions in the Marine Environment, by
888 Multipolarization C- and X- band Synthetic Aperture Radar Data, *Doctoral thesis, The Arctic*
889 *University of Norway, Tromsø, Norway*.

890 Smith, A.J., Flemings, P.B., Fulton, P.M. (2014), Hydrocarbon flux from natural deepwater Gulf
891 of Mexico vents. *Earth and Planetary Science Letters* 395, 241-253.

892 Solomon, E. A., Kastner, M., MacDonald, I. R., Leifer, I. (2009), Considerable methane fluxes to
893 the atmosphere from hydrocarbon seeps in the Gulf of Mexico. *Nature Geoscience*, 2(8), 561-565.

894 Stramma, L., & England M. (1999), On the water masses and mean circulation of the South
895 Atlantic Ocean, *Journal of Geophysical research*, 104, 20863 – 20883.

896 Stramma, L., & Schott, F. (1999), The mean flow field of the tropical Atlantic Ocean. *Deep Sea*
897 *Research Part II: Topical Studies in Oceanography*, 46(1), 279-303.

898 Suresh, G., Heygster, G., Bohrmann, G., Melsheimer, C., Körber, J. H. (2013), An automatic
899 detection system for natural oil seep origin estimation in SAR images. *In 2013 IEEE International*
900 *Geoscience and Remote Sensing Symposium-IGARSS (pp. 3566-3569)*. IEEE.

901 Trivero, P., Biamino, W. (2010), Observing marine pollution with Synthetic Aperture Radar,
902 Observing marine pollution with Synthetic Aperture Radar, *Geosciences and Remote Sensing*,
903 *New Achievements*.

904 Wenau, S., Spiess, V., Pape, T., Fekete, N. (2014 a), Cold seeps at the salt front in the Lower
905 Congo Basin I: Current methane accumulation and active seepage, *Marine and Petroleum*
906 *Geology* (2014), <http://dx.doi.org/10.1016/j.marpetgeo.2014.07.032>.

907 Wenau, S., Spiess, V., Pape, T., Fekete, N. (2014 b), Cold seeps at the salt front in the Lower
908 Congo Basin II: The impact of spatial and temporal evolution of salt-tectonics on hydrocarbon
909 seepage, *Marine and Petroleum Geology* (2014), 1 – 14
910 <http://dx.doi.org/10.1016/j.marpetgeo.2014.09.021>.

911 Williams, A. & Lawrence, G. (2002), The Role of Satellite Seep Detection in exploring the South
912 Atlantic's Ultradeep Water, in Surface exploration case histories: Applications of geochemistry,
913 magnetic, and remote sensing, , Shumacher, D., & LeSchack, L.A., eds., *AAPG Studies in geology*
914 *No. 48 and SEG Geophysical References Series No. 11*, 327-344.

915 Zatyagalova, V.V., Ivanov, A.Y., Gobulov, B.N. (2007), Application of Envisat SAR imagery for
916 mapping and estimation of natural oil seeps in the South Caspian Sea. In *Proceedings of the*
917 *Envisat Symposium 2007*, 23 – 27.

918 Zecchetto, S., della Valle, A., De Biasio, F. (2015), Mitigation of ECMWF–scatterometer wind
919 biases in view of storm surge applications in the Adriatic Sea, *Advances in space Research* 55
920 ,1291 – 1299, <http://dx.doi.org/10.1016/j.asr.2014.12.011>.